Cellular and Molecular Life Sciences (2022) 79:237
https://doi.org/10.1007/s00018-022-04272-8

ORIGINAL ARTICLE

The E3 ubiquitin ligase SMURF2 stabilizes RNA editase ADAR1p110 and promotes its adenosine-to-inosine (A-to-I) editing function

Praveen Koganti[1] · Venkata Narasimha Kadali[1] · Dhanoop Manikoth Ayyathan[1] · Andrea Emanuelli[1] · Biagio Paolini[2] · Gal Levy-Cohen[1] · Michael Blank[1]

Received: 30 August 2021 / Revised: 17 March 2022 / Accepted: 23 March 2022 / Published online: 11 April 2022

Abstract

Epitranscriptomic changes in RNA catalyzed by the RNA-editing enzyme ADAR1 play an essential role in the regulation of diverse molecular and cellular processes, both under physiological conditions and in disease states, including cancer. Yet, despite a growing body of evidence pointing to ADAR1 as a potential therapeutic target, the mechanisms regulating its cellular abundance and activity, particularly of its constitutively expressed and ubiquitous form, ADAR1p110, are poorly understood. Here, we report the HECT-type E3 ubiquitin ligase SMURF2 as a pivotal regulator of ADAR1p110. We show that SMURF2, which is primarily known to promote the ubiquitin-mediated degradation of its protein substrates, protects ADAR1p110 from proteolysis and promotes its A-to-I editase activity in human and mouse cells and tissues. ADAR1p110's interactome analysis performed in human cells also showed a positive influence of SMURF2 on the stability and function of ADAR1p110. Mechanistically, we found that SMURF2 directly binds, ubiquitinates and stabilizes ADAR1p110 in an E3 ubiquitin ligase-dependent manner, through ADAR1p110 ubiquitination at lysine-744 (K744). Mutation of this residue to arginine (K744R), which is also associated with several human disorders, including dyschromatosis symmetrica hereditaria (DSH) and some types of cancer, abolished SMURF2-mediated protection of ADAR1p110 from both proteasomal and lysosomal degradation and inactivated ADAR1p110-mediated RNA editing. Our findings reveal a novel mechanism underlying the regulation of ADAR1 in mammalian cells and suggest SMURF2 as a key cellular factor influencing the protein abundance, interactions and functions of ADAR1p110.

Keywords SMURF2 · ADAR1p110 · Ubiquitination · Interactome · A-to-I RNA editing

Introduction

The hydrolytic deamination of adenosine-to-inosine (A-to-I editing) mediated by adenosine deaminase acting on RNA 1 (ADAR1) can have a significant impact on RNA stability, localization, splicing, siRNA and miRNA biogenesis, as well as protein–protein complex formation and function [1–7]. In addition, it can affect repetitive DNA elements (e.g., *Alu*) and restrict LINE-1 retrotransposition [7–11]. Moreover, although most RNA-editing events occur in introns and 3′UTRs, A-to-I RNA editing in mRNAs can change the protein-coding sequence (the translation machinery reads inosine as guanosine), resulting in the recoding and diversification of gene functions.

There are two distinct ADAR1 proteins found in human cells: ADAR1p150 and ADAR1p110, which are generated from a single gene, *ADAR,* using different promoters and alternative splicing. ADAR1p110 is shorter than the p150 isoform by 295 amino acids due to a protein truncation at the N-terminus. In addition, these proteins exhibit differential expression and, suggestively, differential functions. An interferon (IFN)-inducible ADAR1p150 is mainly a cytoplasmic-sequestered protein whose expression is associated with immune response, whereas a constitutively expressed ADAR1p110 predominantly shows a nuclear localization, although it can also be found in the cytoplasmic compartment of the cell [12–15]. It has been proposed that the differential expression of p110 and p150 isoforms may influence

✉ Michael Blank
michael.blank@biu.ac.il

[1] Laboratory of Molecular and Cellular Cancer Biology, Azrieli Faculty of Medicine, Bar-Ilan University, 1311502 Safed, Israel

[2] Department of Pathology and Laboratory Medicine, IRCCS Fondazione, Istituto Nazionale dei Tumori, Milan, Italy

the editing of RNA targets, as well as affect the editing-independent activities of ADAR1 [15–18]. At the cellular level, ADAR1 has been implicated in the regulation of cell proliferation, differentiation, motility, and antiviral and immune response, as well as cancer growth and metastases [18–24].

Despite significant advances in understanding ADAR1 functions, the mechanisms governing its protein levels and activity, particularly of its constitutively and ubiquitously expressed p110 form, are underexplored. To date, only a limited number of studies have examined the mechanisms associated with ADAR1p110 regulation. These mechanisms include METTL3-mediated methylation of ADAR1 [25], MKK6-p38-MSK MAP kinases and AKT-dependent phosphorylation [15, 26], SUMO-1 conjugation [27], and $SCF^{\beta TrCP}$-mediated ubiquitination and degradation after IFN treatment [28].

In this study, we identify a novel mechanism of ADAR1 regulation. We show that the E3 ubiquitin ligase SMURF2, a ubiquitously expressed protein ligase primarily known for promoting protein degradation [29–37], ubiquitinates and stabilizes ADAR1p110 in a SMURF2 E3 ligase-dependent manner. We further show that SMURF2 promotes ADAR1p110-mediated A-to-I RNA editing, and demonstrate that the stability and activity of ADAR1p110 is regulated through its K744 residue. Our data also show a significant influence of SMURF2 on ADAR1 protein–protein interactions which support the protein stability and functionality of ADAR1p110.

Materials and methods

Cell cultures, reagents and laboratory animals

The cell models used in this study are listed in Supplementary Table 1. Cells were authenticated using a short tandem repeat (STR) profile at the Genomic Center of Biomedical Core Facility (Technion, Israel). All lines, except H1650 cells, were cultured in high glucose DMEM (4.5 g/l D-Glucose, Biological Industries), supplemented with 2 mM L-Glutamine, 10% (v/v) fetal bovine serum (FBS) and 1% (v/v) penicillin–streptomycin (Pen-Strep). H1650 cells were maintained in RPMI-1640 (Biological Industries) supplemented with 2 mM L-Glutamine, 10% (v/v) FBS and 1% (v/v) Pen-Strep. Cells were incubated at 37 °C in a humidified incubator with 5% CO_2.

The proteasomal inhibitor MG-132 was purchased from Merck (Cat# 474790); a lysosomal inhibitor chloroquine (Cat# C6628) and cycloheximide (Cat# 4859) from Sigma; the deubiquitinase inhibitor *N*-ethylmaleimide (NEM) was also obtained from Merck (Cat# 34115).

Smurf2 knockout (KO, $Smurf2^{-/-}$) and control wild-type (WT, $Smurf2^{+/+}$) C57BL/B6 mice were housed at the Faculty SPF animal facility according to FELASA guidelines and experimental protocols approved by the IACUC Committee of Bar-Ilan University (BIU).

Vectors, cloning and site-directed mutagenesis

MYC-SMURF2, FLAG-SMURF2 and GFP-SMURF2 expressing constructs have been previously described [29, 32, 38]. Degron-tagged wild-type SMURF2 (DD-SMURF2) and its catalytically inactive form (C716G, DD-SMURF-2*Mut*) were constructed by PCR using the following primers:

5′-CACCGAATTCATCTAACCCCGGAGGCCGGA-3′ (forward primer, FW, containing EcoRI restriction site) and 5′-ATATCCGCGGTCATTCCACAGCAAATCCACAT-3′ (reverse primer, RV, with SacII restriction site), using the template plasmids pRK1-MYC-SMURF2WT and pRK1-MYC-SMURF2*Mut*. The PCR products were digested with EcoRI and SacII and inserted into pPTuner IRES2 vector (Cat# 631036, Clontech).

The full-length N-terminal FLAG-ADAR1p110 was constructed from the donor vector pcDNA3-ADAR1p110 [39], using the following primers:

5′-CACCTCTAGAGCCGAGATCAAGGAGAAAAT CTG-3′ (forward primer containing XbaI site) and 5′-ATA TAAGATTCTATACTGGGCAGAGATAAAAGTTCT-3′ (reverse primer containing HindIII site). The PCR product was digested with the corresponding restriction enzymes and inserted into pRK2-FLAG vector. Mutations in the constructed pRK2-FLAG-ADAR1p110 vector were introduced by site-directed mutagenesis using the Q5 Site-Directed Mutagenesis Kit (Cat# E0554, NEB) and the following sets of primers:

K7R: FW-5′-ATCAAGGAGAGAATCTGCGAC-3′,
RV-5′-CTCGGCTCTAGAGGATCC-3′;
K279R: FW-5′-GAAGCCAGAGCCAAGGACAGT-3′,
RV-5′-CTCTAGCAGAATTGTCATGGCTT-3′;
K296R: FW-5′-TCCACAGAGAGAGAATCAGAG-3′,
RV-5′-ATAGTGGAATGATTCTTCTGA-3′;
K300R: FW-5′-TCAGAGAGGACTGCAGAGTCC-3′,
RV-5′-TTCTTTCTCTGTGGAATAGTGGGA-3′;
K342R: FW-5′-TCCTCGCCAGAGAAGGCCCTGC-3′,
RV-5′-GACGGAATTCGCAGGAGTTCCC-3′;
K374R: FW-5′-AAAGTGGCAAGGCAGATGGCC-3′,
RV-5′-CTTGCTGGGAGCACTCACACT-3′;
K503R: FW-5′-AGAACGAGAGGGCAGAACGCAT-3′,
RV-5′-CCCCAATCAAGACACGGAGAGC-3′;
K600R: FW-5′-CGCTGTGTGAGAGGAGATTCT-3′,
RV-5′-ATTCCCTGTTCCCAAGCT-3′;
K649R: FW-5′-GAACCTGCTAGGGGAGGAGAAAA-3′,
RV-5′-AAATATACTATCCTTCGCAGTCTGGGA-3′;

K653R: FW-5′-GGAGGAGAAAGGCTCCAAATAAAA-3′,
RV-5′-CTTAGCAGGTTCAAATATACTACC-3′;
K704R: FW-5′-AAACAAGGAAGGCTCCGCACC-3′,
RV-5′-GGGATTCTCGAAGACAGGGTA-3′;
K744R: FW-5′-TGTAGTGACAGAATCCTACGCTGG-3′,
RV-5′-GGACATGGTACGGAGTCTCTC-3′;
K820R: FW-5′-TATGATTCCAGAAGGCAATCCGGG-3′,
RV-5′-TATGCTGACTCTGCCAACCTTGGG-3′.

ADAR1p110-WT, K296R, K744R and deaminase-inactive (H615Q/E617A) mutants were also cloned into a pcDNA3-FLAG vector. The primers used to generate the pcDNA3-FLAG-ADAR1p110WT, K296R and K744R constructs are listed as follows:

FW: 5′-CACCGGATCCGCCGAGATCAAGGAGAAAATCTG-3′;
RV: 5′-ATATCTCGAGCTATACTGGGCAGAGATAAAAGTTCT-3′.

The primers used to generate the pcDNA3-FLAG-ADAR1p110-H615Q/E617A construct are:

FW: 5′-CACCGGATCCGCCGAGATCAAGGAGAAAATCTG-3′;
RV: 5′-ATATCTCGAGCTAATGGTGATGGTGATGATGTACT-3′.

All constructs were sequence-verified.

Cell transfections and generation of stable cell lines

For transient protein expression in HEK-293T cells, we used either polyethylenimine (Cat# 408727, Sigma) or FuGENE®6 (Cat# E2692, Promega); for U2OS and HeLa cells—FuGENE®6 and FuGENE® HD (Cat# E2311, Promega), respectively. To generate stable cell lines expressing SMURF2WT and *Mut* proteins (GFP- and DD-tagged), U2OS cells were transfected using FuGENE® 6 and maintained in 550 µg/ml of G418 (Cat# 345810, Merck) for at least 2 weeks. To obtain a homogenous population of positive fluorescent cells, the samples were also sorted using the MoFlo Astrios cell sorter (Beckman Coulter). To generate U2OS cells expressing FLAG-SMURF2WT or an empty FLAG vector, we used the pBabe-FLAG-SMURF2-puro-based retroviral system, as previously described [29, 38].

RNAi and *SMURF2*^{CRISPR} cells

Predesigned Dicer-substrate siRNA (DsiRNA) duplexes targeting *SMURF2*, *ADAR1* and non-silencing (NS) control siRNAs were purchased from Integrated DNA Technologies (IDT).

siNS: 5′-CGUUAAUCGCGUAUAAUACGCGUAT-3′;
si*SMURF2*-#1 (3′UTR): 5′-GCAGAGUUUCAAAGAAUAUGCUGAA-3′;
si*SMURF2*-#2 (CDS): 5′-AGUUAAUCCGGAACAUUUAUCCUAT-3′;
si*ADAR1*: 5′-GGCAGAAACCUAAGAAGUUAUCUTT-3′.

Cells were transfected with the corresponding siRNA using Oligofectamine (Cat# 12252011, Invitrogen) according to manufacturer's instructions, and analyzed 72 h after transfection. *SMURF2* knockdown stable cells were generated by infecting the cells with lentiviruses containing pLKO.1-SMURF2-puro vector [38, 40], followed by selection with puromycin (1–2 µg/ml) for 2 weeks. The shRNA targeting luciferase gene (shLuc) served as a control. *SMURF2*^{CRISPR} cells were generated by using the CRISPR/Cas9 genome editing tool (Cat# KN210866, Origene), as described [41].

Protein extraction, western blot analysis and immunoprecipitation

Whole cell lysates (WCL) were prepared by disrupting the cell pellet in RIPA buffer (50 mM Tris–HCl [pH 7.8], 1% Nonidet P40 Substitute, 150 mM NaCl, 0.1% SDS, 0.5% sodium deoxycholate), followed by incubation on ice (30 min), sample sonication (30% amplitude, 1 min on ice) and centrifugation (14,000 rpm, 15 min, 4 °C). For protein extraction from mouse tissues, the samples were homogenized in RIPA buffer using TissueRuptor II (Qiagen), followed by sonication (30% amplitude, 1 min on ice), and cleared by centrifugation (14,000 rpm, 20 min, 4 °C). All lysis buffers were supplemented with a protease inhibitor cocktail (Cat# 11836153001, Roche) and phosphatase inhibitor cocktails (Cat# P5726 and Cat# P0044, Sigma). Protein concentrations were assessed using the Pierce™ BCA Assay kit (Cat# TS-23227, Thermo Fisher Scientific). Samples were subjected to SDS-PAGE and subsequently transferred to a PVDF membrane (Cat# 10600023, GE Healthcare), followed by incubation with the indicated primary and corresponding secondary antibodies (Supplementary Table 2). The membranes were visualized in the SyngeneG:BOX. Quantification of the data obtained in Western blot analysis was conducted using Gel.Quant.NET, relatively to the loading controls.

For immunoprecipitation/co-immunoprecipitation (IP/co-IP) of endogenous proteins, cells were lysed using different lysis conditions: 0.5% NP-40 buffer (0.5% Nonidet P40 Substitute, 25 mM Tris–HCl [pH 7.5], 137 mM NaCl, 1 mM EDTA, 1 mM EGTA, 5% glycerol); 1% NP-40 buffer (1% Nonidet P40 Substitute, 25 mM Tris–HCl [pH 7.5], 137 mM NaCl, 1 mM EDTA, 1 mM EGTA, 5% glycerol); or using a freeze-thawing buffer (600 mM KCl, 20 mM Tris–HCl [pH 7.8], 20% glycerol), followed by sample resuspension in the dilution buffer (45 mM Tris–HCl [pH 7.8], 2.25 mM EDTA, 0.1% Nonidet P40 Substitute), as described [38]. Cell lysates were then incubated overnight at 4 °C with anti-SMURF2 antibody (Cat# sc25511; Santa Cruz) or rabbit IgG as a control (Cat# I5006; Sigma). Protein-G Sepharose beads (4 Fast Flow, Cat# 17–0618-01, GE Healthcare) were then added and samples were incubated for an additional 2 h at 4 °C under rotation. Subsequently, beads were washed several times with an ice-cold lysis buffer and boiled for 5 min in 5× SDS sample buffer (50 mM Tris–HCl [pH 8], 5 mM EDTA, 5% SDS, 50% glycerol, 50 mM Dithiothreitol (DTT), 0.05% w/v bromophenol blue, 6% β-mercaptoethanol).

For IP/co-IP of recombinant proteins, WCL were obtained using 1% NP-40 lysis buffer, followed by samples' incubation on ice for 30 min and centrifugation (14,000 rpm, 4 °C, 15 min). Subsequently, FLAG-tagged proteins were IPed using anti-FLAG resin (anti-FLAG®M2 affinity gel, Cat# A2220, Sigma); MYC- and GFP-tagged proteins were IPed using anti-MYC (Cat# sc-40, Santa Cruz) and anti-GFP (Cat# 11814460001, Roche) antibodies, respectively. The IPs were then recovered and analyzed as described above.

Immunofluorescence (IF), proximity ligation assay (PLA), confocal and stimulated emission depletion (STED) microscopy

These analyses were carried out as previously described [32, 38, 40], using the following set of primary and paired secondary antibodies: anti-ADAR1 (Cat# HPA003890, 1:150, Sigma) and Rhodamine Red™X conjugated goat anti-rabbit IgG (Cat# 111-296-045, 1:200, Jackson ImmunoResearch Laboratories); anti-FLAG (Cat# F3165, 1:1000, Sigma) and Rhodamine Red™X fluorophore goat anti-mouse IgG (Cat# 115-296-071, 1:200, Jackson ImmunoResearch Laboratories). DNA was counterstained with Hoechst 33258 (Cat# B2883, Sigma) and the coverslips were mounted onto glass slides with ProLong® Diamond Antifade Mountant (Cat# P36961, Invitrogen).

For PLA, we used anti-ADAR1 (Cat# HPA003890, 1:150, Sigma) and anti-GFP (Cat# 11814460001, 1:200, Roche) antibodies, followed by the use of Duolink™ in situ red starter kit (Cat# DUO92101, Sigma). Confocal microscopy images were visualized and captured using a LSM780 Inverted Confocal Microscope (Zeiss) fitted with Plan-Apochromat 63×/1.40 Oil DIC M27 objective. For colocalization analysis, at least 8–10 different fields (with 5–10 cells per field) were acquired. All comparative images were obtained under identical microscope and camera settings, and analyzed using ZEN software (Zeiss). The results were quantified using Fiji software [42].

For STED super-resolution microscopy, U2OS cells expressing GFP-SMURF2 were seeded on coverslips precoated with poly-D-lysine (Cat# P7280, Sigma). Subsequently, the samples were stained using an anti-ADAR1 antibody (Cat# HPA003890, 1:150, Sigma) and a Rhodamine Red™X conjugated goat anti-rabbit IgG (Cat# 111-296-045, 1:200, Jackson ImmunoResearch Laboratories). STED images were captured using a Leica SPi 8 Super-Resolution gSTED Inverted Confocal Microscope fitted with HC PL APO 100×/1.40 Oil objective, and analyzed using Leica Application Suite X software.

Immunohistochemistry (IHC)

This analysis was conducted as described [29, 43], with some modifications. In brief, human normal tissue microarrays (TMAs), containing 32 types of normal tissues taken from three individuals, were purchased from US Biomax, Inc (Cat# FDA999m; http://www.biomax.us/FDA999m). Mice tissues were fixed in 4% PFA by intracardial perfusion and processed for paraffin block preparation. Thereafter, 5 µm tissue sections were cut using a Leica RM2235 microtome and collected on superfrost microscope slides. *Smurf2*KO and littermate WT control tissues were layered on the same slide in order to obtain uniform staining. Slides were deparaffinized in xylene and hydrated in a descending scale of ethanol. Antigen retrieval was performed for 10 min in 10 mM citrate buffer [pH 6.0], using a microwave oven. Sections were then washed with 1× PBS and treated with 3% H_2O_2 for 25 min to inactivate endogenous peroxidases. Subsequently, the samples were blocked and stained with Vectastain Elite ABC kit (Rabbit IgG, Cat# PK-6101, Vector Lab), according to manufacturer's instructions. Primary antibodies: ADAR1 (Cat# HPA003890, 1:800, Sigma) and SMURF2 (Cat# sc25511, 1:100, Santa Cruz) were incubated overnight on tissue samples at 4 °C. Samples were then washed and incubated with DAB substrate peroxidase (HRP) kit (Cat# SK-4100, Vector Lab), counterstained with hematoxylin (Cat# H-3502, Vector Lab), dehydrated and mounted with coverslips using VectaMount™ permanent mounting medium (Cat# H-5000, Vector Lab). Histological images were taken using an Axio Imager M2 microscope (Zeiss) through a Plan-Apochromat 20×/0.8 M27 objective. All comparable samples were sampled on the same slide, and all staining procedures were done on slides positioned horizontally. Image analysis was conducted using ZEN software.

Histological evaluations and TMA scoring were carried out by an experienced pathologist, Dr. Biagio Paolini, at the Istituto Nazionale dei Tumori (Italy). Scoring for SMURF2 and ADAR1 staining was performed using the standard scoring system (0 = < 10%; 1 = 10–24%; 2 = 25–49%; 3 = 50–74%; 4 = 75–100%) [29].

Protein production and purification

GST-SMURF2WT and *Mut* proteins were produced in *E.coli* and purified using Glutathione Sepharose™ 4B beads (Cat# 17075601, GE Healthcare) [38]. Untagged SMURF2 proteins were generated by the cleavage of purified GST-SMURF2 with TEV protease. FLAG-ADAR1p110 was produced using the TnT® SP6 high-yield wheat germ expression system (Cat# L3260, Promega). Note that, similar to mammalian cells, this expression system contains inositol hexakiphosphate (IP6, also known as a phytic acid) [44, 45], which is considered necessary for the correct conformation and function of ADAR proteins [46, 47]. In addition, FLAG-ADAR1p110 was produced in and affinity-purified from HEK-293T cells, using an approach described in [40], with several modifications. In brief, cells transiently expressing FLAG-ADAR1p110 were lysed using an NP-40 lysis buffer (0.5% Nonidet P40 Substitute, 25 mM Tris–HCl [pH 7.5], 150 mM NaCl), supplemented with 5 μM ZnSO4 and EDTA-free protease inhibitors (Cat# 11836170001, Roche). The samples were then mechanically disrupted by passing through a 29 g needle, incubated on ice and centrifuged. The obtained supernatants were incubated overnight with anti-FLAG® M2 affinity gel at 4 °C, washed four times with a lysis buffer and resuspended in PBS for subsequent in vitro (in tube) ubiquitination analysis. For in vitro binding experiments, the gel resin was first washed twice with a harsh washing buffer (10 mM Tris–HCl [pH 8], 1 M NaCl, and 1% Nonidet P40 Substitute), followed by two additional washes with an elution buffer (50 mM HEPES [pH 7.3], 250 mM NaCl, 0.5% Nonidet P40 Substitute, 5 μM ZnSO4). FLAG-ADAR1p110 was then eluted from the beads using 3 × FLAG peptide (F4799, Sigma). The purity of the proteins was assessed using PageBlue/Coomassie protein staining (Cat# 24620; Thermo Fischer Scientific).

In vitro protein binding and pull-down assays

These assays were conducted as described [32, 38], with a few adjustments. Briefly, for GST pull-down assays, FLAG-ADAR1p110 was coincubated with either GST or GST-SMURF2 in a binding buffer (50 mM Tris–HCl [pH 7.5], 120 mM NaCl, 2 mM EDTA and 0.1% Nonidet P40 Substitute) at 37 °C for 15 min. GST proteins were then pulled-down using Glutathione Sepharose™ 4B beads, washed several times with an ice-cold binding buffer and eluted from beads using a 5 × SDS sample buffer. For ADAR1 pull-down, FLAG-ADAR1p110 was coincubated with untagged SMURF2 in binding buffer at 37 °C for 15 min. Subsequently, FLAG-ADAR1p110 was pulled-down using anti-FLAG resin. In addition, FLAG-ADAR1p110 was coincubated with SMURF2WT and *Mut* proteins, with subsequent pull-down of SMURF2 using anti-SMURF2 antibody (Cat# sc25511, Santa Cruz).

We also examined the interaction between GST-SMURF2 (WT and *Mut*) and FLAG-ADAR1p110 produced in and affinity-purified from HEK-293T cells (described in the previous section). These proteins were coincubated in binding buffer (50 mM Tris–HCl [pH 7.5], 120 mM NaCl, 0.1% Nonidet P40 Substitute, 5 μM ZnSO4) at 4 °C for 30 min, followed by GST-SMURF2 pull-down. The complex formation between GST-SMURF2 and FLAG-ADAR1p110 was analyzed by Western blotting.

In vitro and in cellulo ubiquitination assays

These assays were carried out as we previously described [32, 40, 48], with several modifications. For in cellulo ubiquitination assay, cells were lysed in RIPA buffer supplemented with 5 mM NEM, or in 1% SDS followed by immediate sample boiling at 95 °C (15 min). NEM was added to the lysis buffer to preserve proteins in the ubiquitination state, at which they were present in the intact cells [49]. Subsequently, the samples lysed in 1% SDS buffer were diluted with SDS-free RIPA buffer (containing 5 mM NEM) to reduce SDS concentration down to 0.1%. Cell extracts were then kept on ice for 30 min and sonicated (30% amplitude, 1 min on ice). FLAG-ADAR1p110 or endogenously expressed ADAR1 were IPed using anti-FLAG (Cat# A2220, Sigma) or anti-ADAR1 antibodies (Cat# A303-884A, Bethyl Laboratories), respectively. For the ubiquitin chain formation assay, FLAG-ADAR1p110 was coexpressed in HEK-293T cells together with MYC-SMURF2 (or an empty MYC vector as an additional control) and either ubiquitin wild-type (HA-Ubiquitin-WT) or its different mutant forms (obtained from Addgene): K6-only (Cat# 22900), K11-only (Cat# 22901), K27-only (Cat# 22902), K29-only (Cat# 22903), K33-only (Cat# 17607), K48-only (Cat# 17605) and K63-only (Cat# 17606). These mutants can form ubiquitin chains only through the indicated lysine residues; all other ubiquitin lysines were mutated to arginines. K6, K11, K27, and K29 mutants were a gift from Sandra Weller; K33, K48 and K63 mutants were a gift from Ted Dawson. Cells were then lysed and ADAR1p110 ubiquitination was analyzed as described above.

For the in vitro ubiquitination assay, we used both affinity-purified FLAG-ADAR1p110 and MYC-ADAR1p110 purchased from Origene (Cat# TP319761). FLAG-ADAR1p110, immobilized on M2 affinity resin, was

incubated with 250 ng of GST or GST-SMURF2 (WT or *Mut*), 10 µg HA-ubiquitin (Cat# U-110, Boston Biochem), 200 ng of ubiquitin-activating enzyme E1 (UBE1, Cat# E-305, Boston Biochem), 300 ng of ubiquitin-conjugating enzyme E2 (UbcH5c, Cat# E2-627, Boston Biochem) and 2 mM Mg-ATP (B-20, Boston Biochem) in an E3 ligase reaction buffer (Cat# B-71, Boston Biochem) for 2 h at 37 °C. The beads were then washed four times with an ice-cold wash buffer (0.5% Nonidet P40 Substitute, 25 mM Tris–HCl [pH 7.5], 150 mM NaCl, 5 µM ZnSO4 and EDTA-free protease inhibitors). ADAR1p110 was released from the beads using 5 × SDS sample buffer.

A similar reaction was also conducted with purified MYC-ADAR1p110 obtained from Origene. The reaction contained 100 ng E1, 150 ng E2, 250 ng of GST-SMURF2 (as an E3 ligase), 350 ng of MYC-ADAR1p110 (a substrate), 5 µg HA-ubiquitin and 1 mM Mg-ATP. The reaction was carried out as described above and stopped with an ice-cold RIPA buffer supplemented with 5 mM NEM. MYC-ADAR1p110 was then IPed using anti-MYC antibody and Protein-G Sepharose beads. The beads were washed several times with an ice-cold RIPA buffer and MYC-ADAR1p110 was eluted from the beads using 5 × SDS sample buffer. The ubiquitination of ADAR1p110 was analyzed in immunoblots using anti-HA (ubiquitin) antibody (1:1000, Cat# 715500, Thermo Fisher Scientific).

Identification of SMURF2 ubiquitination sites on ADAR1p110

HEK-293T cells were cotransfected with MYC-vectors (Empty, SMURF2WT or SMURF2*Mut*), FLAG-ADAR1p110 and HA-Ubiquitin. Twenty-six hours post transfection, cells were lysed using RIPA buffer supplemented with 5 mM NEM, following by IP with anti-FLAG resin. FLAG-ADAR1p110 was then eluted from beads using 3 × FLAG peptide. To generate peptides prior to the mass spectrometry (MS) analysis, a filter-aided sample preparation (FASP) method was used [40]. In brief, the eluates were first purified with a 10 kDa cutoff filter unit and the membranes were washed with a digestion buffer (50 mM Tris pH 8.0). DTT was then added to reduce the disulfide bonds, and the filters were washed with a digestion buffer, followed by the addition of a NEM buffer (0.1 M NEM in digestion buffer) and another sample washing with a digestion buffer. Subsequently, proteins were digested using a sequence-grade modified trypsin (Cat# V5111, Promega) at a ratio of FLAG-ADAR1 to trypsin 10:1 (w/v) and incubated overnight at 37 °C. The following day, the digested samples were washed twice with 0.5 M NaCl and desalted using TopTip (Cat# TT1C18, Glygen). The samples were then vacuum dried and reconstituted with IAP buffer (50 mM MOPS [pH 7.2], 10 mM sodium phosphate, 50 mM NaCl). Subsequently, PTMScan® Ubiquitin Branch Remnant Motif (K-ε-GG) beads (Cat# 5562, Cell Signaling Technology) were added, and samples were incubated overnight at 4 °C under rotation. The following day, the K-ε-GG beads were washed twice with 0.25% Nonidet P40 substitute in IAP buffer, twice with IAP and then twice with MS-grade water. The peptides were eluted in low pH 0.15% trifluoroacetic acid and vortexed at low speed for 10 min. Finally, the samples were desalted again using NuTip (Cat# NT2C18, Glygen), lyophilized and sent for the LC–MS/MS analysis at the Smoler Protein Research Centre (Technion, Israel). The data obtained from MS were analyzed using MaxQuant.

RNA editing

RNA editing was performed as previously described [50], with some modifications. Briefly, HEK-293T and HeLa cells were transfected with either FLAG-ADAR1p110-WT or its mutant forms. Total RNA was isolated from cells 24 h or 48 h after transfection using the RNeasy Mini Kit (Cat# 74104, Qiagen), reverse-transcribed with random primers using the High Capacity cDNA Reverse Transcription Kit (Cat# 4368814, Applied Biosystems) and treated with DNase I (Cat# 79256, Qiagen) to remove possible contamination with genomic DNA. Human filamin B (*FLNB*) and antizyme inhibitor 1 (*AZIN1*) editing regions were amplified with specific primers using Q5 High-Fidelity 2 × Master Mix (Cat# MO492S, NEB), purified using Wizard SV Gel and PCR Clean-Up System (Cat# A9281, Promega) and subjected to Sanger sequencing with the corresponding FW primers. Editing levels were assessed in the chromatograms by measuring peak heights using BioEdit and calculated as a ratio of G-peak height to A + G-peak height (G/G + A).

FLNB primers: FW: 5′-TGAGTTCAGCATTTGGACC-3′;
RV: 5′-GAATTCCGACTGGATACCT-3′.
AZIN1 primers: FW: 5′-TCGCAGTTAATATCATAG C-3′;
RV: 5′-AAGGCACAAAGAAGAAGT-3′.

In addition, we assessed RNA editing of *Flnb* [51] and *Azin1* [52] transcripts in *Smurf2*KO and corresponding WT mouse tissues, using the following sets of primers:

Flnb: FW: 5′-CCACGGTTGGCAGTATCTGT-3′;
RV: 5′-TAGGCTGACACTAGAGCAGGA-3′.
Azin1: FW: 5′-TTCTGCGTTTACACTTGCAGTCA-3′;
RV: 5′-AGCTGAATACAAGAGGGTGCAA-3′.

Flnb PCR product was sequenced with its RV primer; *Azin1* with its FW primer. *FLNB/Flnb* and *AZIN1/Azin1* PCR products were verified on an agarose gel prior to sample sequencing.

RT-qPCR

Total RNA was reverse-transcribed with random primers using the High Capacity cDNA Reverse Transcription Kit (Applied Biosystems). ADAR1 cDNA levels were then determined using the Fast SYBR Green Master mix (Cat# 4385612, Applied Biosystems) and ViiA™ 7 Real-Time PCR System (Cat# 4374966, Thermo Fisher Scientific). The experiments were performed three times with three technical replicates for each experiment. The gene expression was calculated using the $2^{-\Delta\Delta Ct}$ method and normalized to the *HGPRT* gene. The following PCR primers were used:

for *ADAR1*: FW: 5′-GGCAGCCTCCGGGTG-3′;
RV: 5′-CTGTCTGTGCTCATAGCCTTGA-3′;
for *HPRT1*: FW: 5′-TTGCTTTCCTTGGTCAGGCA-3′;
RV: 5′-ATCCAACACTTCGTGGGGTC-3′.

These primers were designed for exon–exon spanning and tested for efficiency through the standard curve.

ADAR1 interactome analysis

Cells were transduced with the indicated vectors and constructs, and lysed in 1% NP-40 lysis buffer supplemented with protease and phosphatase inhibitors. The lysates were then pre-cleared with Protein A/G PLUS agarose beads (Cat# sc-2003, Santa Cruz) for IP-FLAG samples or with Protein-G Sepharose beads for IP-MYC samples. FLAG-ADAR1p110 was IPed using anti-FLAG resin; MYC-tagged proteins were IPed using anti-MYC antibody followed by pull-down with Protein-G-Sepharose beads. After washing beads (three times) in a pre-urea wash buffer (50 mM Tris [pH 8.5], 1 mM EGTA, and 75 mM KCl), proteins were eluted in an 8 M Urea buffer (8 M Urea, 20 mM Tris [pH 7.5], 100 mM NaCl) and submitted to MS analysis. The resulting peptides were annotated with the Discoverer™ software tool against the human proteome database and two search algorithms: Sequest (Thermo Fisher Scientific) and Mascot (Matrix Science). All identified peptides were filtered with high confidence (False Discovery Rate (FDR) ≤ 1%), top rank and mass accuracy. Protein classification was performed using the PANTHER platform [53]. The subcellular localization of identified ADAR1 interactors was analyzed using UniProtKB. In both PANTHER and UniProtKB analyses, we selected proteins whose abundance changed in the presence of SMURF2 by at least twofold. Protein–protein interaction network was reconstructed using the STRING 11.0 tool [54]. Only interactors that are connected within the network were considered, and k-means clustering method was applied to classify proteins into different categories. Gene Ontology (GO) terms analysis was carried out using the ToppFun suite bioinformatics tool [55] at https://toppgene.cchmc.org/. GO terms with Benjamini and Hochberg adjusted FDR (q-value FDR B&H) < 0.05 were considered significant.

Statistical analysis

A two-tailed Student's *t* test was applied for statistical analysis of normally distributed data (using the Excel analysis tool pack); Mann–Whitney *U* test (using GraphPad Prism, version 7.04) was used for analysis of data that was not normally distributed (PLA and IF analysis of ADAR1 protein expression in HeLa cells). Data with *P*-values of ≤ 0.05 were considered as statistically significant.

Results

SMURF2 physically interacts with ADAR1

The initial clue indicating a potential interaction between SMURF2 and ADAR1 was obtained in our unpublished preliminary study of SMURF2 interactors in HeLa cells. To further investigate the possibility of a complex formation between SMURF2 and ADAR1, we coexpressed FLAG-ADAR1p110 and MYC-SMURF2 in HEK-293T cells, IPed these proteins with the corresponding antibodies, and submitted the samples to MS analysis. Using this approach, we identified a reciprocal interaction between ADAR1p110 and SMURF2 (Supplementary Fig. 1A, B). Specifically, we found 65 SMURF2-specific peptides associated with FLAG-ADAR1p110 vs. zero peptides in cells coexpressing FLAG-ADAR1p110 and MYC-Empty vector (Supplementary Fig. 1A, upper left panel). Correspondingly, the area under the peak of the peptides (a measure of a protein abundance) for SMURF2 was markedly increased in FLAG-ADAR1p110/MYC-SMURF2 coexpressing samples (Supplementary Fig. 1A, upper right panel). The abundance of ADAR1 peptides detected in samples coexpressing FLAG-ADAR1p110/MYC-Empty and FLAG-ADAR1p110/MYC-SMURF2 was comparable, with a similar number of ADAR1 peptides detected in these samples: 170 and 171 peptides, respectively (Supplementary Fig. 1A, bottom panels). The interaction between FLAG-ADAR1 and MYC-SMURF2 was also detected in the MS analysis of samples IPed with anti-MYC antibody (Supplementary Fig. 1B).

Subsequent co-IP analysis of MYC-SMURF2 and FLAG-ADAR1p110 in HEK-293T cells affirmed the reciprocal interactions between these proteins. The results also showed that ADAR1p110 can interact with both SMURF2 wild-type and its catalytically inactive form, SMURF2*Mut* (Fig. 1A and Supplementary Fig. 1C). The co-IP analysis of endogenous proteins provided further supportive evidence for a complex formation between SMURF2 and ADAR1p110

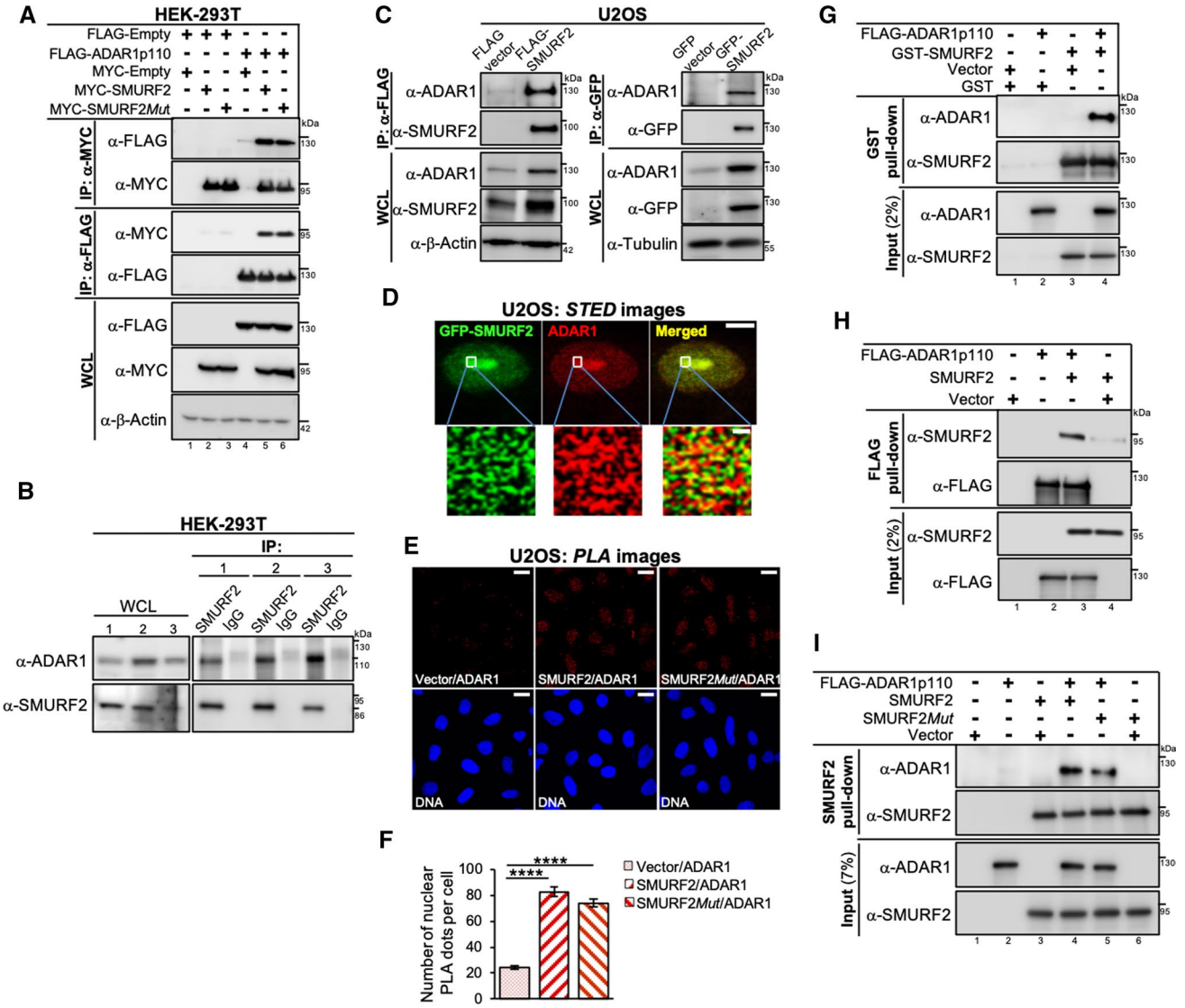

Fig. 1 SMURF2 physically interacts with ADAR1p110. **A** Reciprocal co-IPs showing interactions between MYC-SMURF2 and FLAG-ADAR1p110 in HEK-293T cells. Proteins were released from the beads using an 8 M urea elution buffer. WCL, whole cell lysates. **B** co-IP analysis showing interaction between endogenous SMURF2 and ADAR1 under various lysis conditions: #1—lysed with a buffer containing 0.5% NP-40; #2—1% NP-40; #3—600 mM KCL, no detergent (freezing–thawing buffer). **C** co-IPs showing interactions between either FLAG- or GFP-SMURF2 and endogenous ADAR1 in U2OS cells. **D** STED microscopy images showing colocalization of GFP-SMURF2 and ADAR1 in the U2OS cell nucleus. Scale bar: 5 µm. White rectangles mark the area detailed under the STED microscopy. Scale bar in the bottom images: 0.2 µm. **E** PLA images showing the sites of interactions between GFP-SMURF2 and ADAR1 in U2OS cells (red fluorescence spots). Scale bar: 20 µm. **F** Quantifications of the PLA data on SMURF2–ADAR1 interaction in U2OS cell nuclei. 100 cells/sample. Data are mean ± SEM. ****$P \leq 0.0001$. **G** In vitro binding assay (GST pull-down) showing direct interaction between GST-SMURF2 and FLAG-ADAR1p110. **H** In vitro binding assay (FLAG pull-down) showing the interaction between FLAG-ADAR1p110 and untagged SMURF2. **I** In vitro binding assay showing that both SMURF2 wild-type and its catalytically dead mutant (SMURF2*Mut*) are capable of interacting directly with ADAR1p110

(henceforward ADAR1), and indicated that this interaction is stable under different lysis conditions (Fig. 1B).

The interaction between SMURF2 and ADAR1 was not limited to HEK-293T cells and was observed also in other types of cells, including U2OS and HeLa cells (Fig. 1C and Supplementary Fig. 1D–H). Using a U2OS cell model, we demonstrate that the ability of SMURF2 to interact with ADAR1 does not depend on the size of molecular tag attached to SMURF2: FLAG or GFP (Fig. 1C). Furthermore, the confocal laser-scanning microscopy (CLSM) analysis indicated that SMURF2 and ADAR1 colocalize in both interphase and mitotic cells, suggesting that these proteins interact throughout the cell division cycle (Supplementary Fig. 1D, E). The Z-stack analysis confirmed the

colocalization between SMURF2 and ADAR1, and indicated that ADAR1 colocalizes with both active and inactive forms of SMURF2 (Supplementary Fig. 1F, G), corroborating the results obtained in our biochemical experiments.

To determine if the interaction between ADAR1 and SMURF2 is direct, we performed several lines of investigation. First, we carried out a super-resolution STED microscopy analysis, which indicated that ADAR1 and SMURF2 colocalize within the nanometer scale range (Fig. 1D). Then, we conducted a proximity ligation assay, which enables the visualization of protein–protein interactions at a distance of less than 40 nm [56]. The obtained results (Fig. 1E, F) indicated a direct interaction between ADAR1 and SMURF2. Finally, we performed in vitro binding assays which included SMURF2 (GST-tagged and untagged) and FLAG-ADAR1, produced either in HEK-293T cells or using a wheat germ expression system. The results obtained in these binding assays confirmed that SMURF2 and ADAR1 interact with each other in a direct manner (Fig. 1G–I and Supplementary Fig. 1J). The data also showed that ADAR1p110 directly interacts with both SMURF2 wild-type and its E3 ligase-dead form–SMURF2^{C716G} (Fig. 1I, lanes 4 and 5, and Supplementary Fig. 1J, lanes 2 and 3), supporting our other results obtained in co-IP and colocalization studies.

SMURF2 directly ubiquitinates ADAR1

To examine if SMURF2 acts as an E3 ubiquitin ligase of ADAR1, we first conducted in cellulo ubiquitination assays in which FLAG-ADAR1p110 was coexpressed with MYC-SMURF2, or with MYC-SMURF2*Mut*, and HA-Ubiquitin. Cells transfected with an empty MYC vector served as an additional control. FLAG-ADAR1p110 was then IPed using anti-FLAG resin and its ubiquitination pattern analyzed with an anti-HA antibody that recognizes HA-Ubiquitin conjugated to FLAG-ADAR1p110 (Fig. 2A, lanes 3–5 vs. 1–2). The results showed that SMURF2 ubiquitinates ADAR1 in an E3 ligase-dependent manner (Fig. 2A, B). This effect was consistently observed under different lysis conditions, and was particularly notable at molecular sizes ranging between ~ 130 and 250 kDa, suggesting that, in cells, SMURF2 mostly oligo-ubiquitinates ADAR1. SMURF2-mediated ubiquitination of the endogenously expressed ADAR1 was also evident (Supplementary Fig. 2A).

Subsequently, experiments conducted with the ubiquitin mutant (ubiquitin-KO), wherein all lysine residues were mutated to arginines, supported the SMURF2-mediated oligoubiquitination of ADAR1 (Fig. 2C, D). Furthermore, using different ubiquitin mutants, we found that SMURF2 modulates/facilitates the formation on ADAR1 of heterotypic ubiquitin chains, involving different ubiquitin lysine residues, with the exception of lysine-33 (Supplementary Fig. 2B).

Finally, we conducted in vitro ubiquitination reactions in a tube, using purified components of the ubiquitin-transferring machinery (described in the "Materials and methods" section), and incorporating SMURF2 (as an E3 ubiquitin ligase) and ADAR1p110 as a substrate. The obtained results clearly showed that SMURF2 is capable of directly ubiquitinating ADAR1, and demonstrated the dependence of this phenomenon on the catalytic activity of SMURF2 (Fig. 2E, F and Supplementary Fig. 2C, D).

SMURF2 positively regulates ADAR1 protein expression, protecting it from degradation

In our protein binding experiments, we noted that the adventitious expression of SMURF2 in U2OS cells increased ADAR1 protein abundance, an effect that was consistently seen in different settings (Fig. 1C and Supplementary Fig. 3A, B). To further explore this phenomenon, we first examined the effects of SMURF2 on the expression of ADAR1 in cells engineered to carry out the inducible form of SMURF2 (DD-SMURF2). The induction of DD-SMURF2 was achieved by adding to the cells of a specific ligand, Shield-1, which stabilizes SMURF2 through the inactivation of its destabilization domain (DD). Using this system, we found that ADAR1 protein levels are highly sensitive to changes in the expression levels of SMURF2 (Fig. 3A and Supplementary Fig. 3C). Moreover, the results showed that unaltered catalytic activity of SMURF2 is required for this phenomenon, as the enzymatically dead SMURF2 (DD-SMURF2*Mut*) failed to heighten ADAR1 expression (Fig. 3B, C). Similar results were also observed in cells expressing a GFP-tagged version of SMURF2 (Fig. 3D).

Conversely, the knockdown of *SMURF2*, either through *SMURF2*-specific siRNA or CRISPR/Cas9 gene-editing (*SMURF2*^{CR}), substantially reduced the protein levels of ADAR1 (Fig. 3E and Supplementary Fig. 3D). The decreased protein abundance of ADAR1 after *SMURF2* knockdown was monitored in different cell models, including cervical, lung, breast and prostate, upon both acute and stable depletion of *SMURF2* with either siRNA or lentiviral-based shRNAs, respectively (Fig. 3F).

RT-qPCR analysis showed that ADAR1 mRNA levels were unaffected by SMURF2 depletion, suggesting that SMURF2 regulates ADAR1 posttranscriptionally/posttranslationally (Supplementary Fig. 3E, F). The posttranslational level of ADAR1 regulation by SMURF2 was further corroborated in cells following treatment with the proteasomal inhibitor MG-132 and lysosomal inhibitor chloroquine (CQ), which restored the protein levels of ADAR1 close to the levels observed in control cells (Fig. 3G, lanes 4 vs. 1).

To relate these findings to the physiological settings in vivo, we then analyzed the expression of ADAR1 in

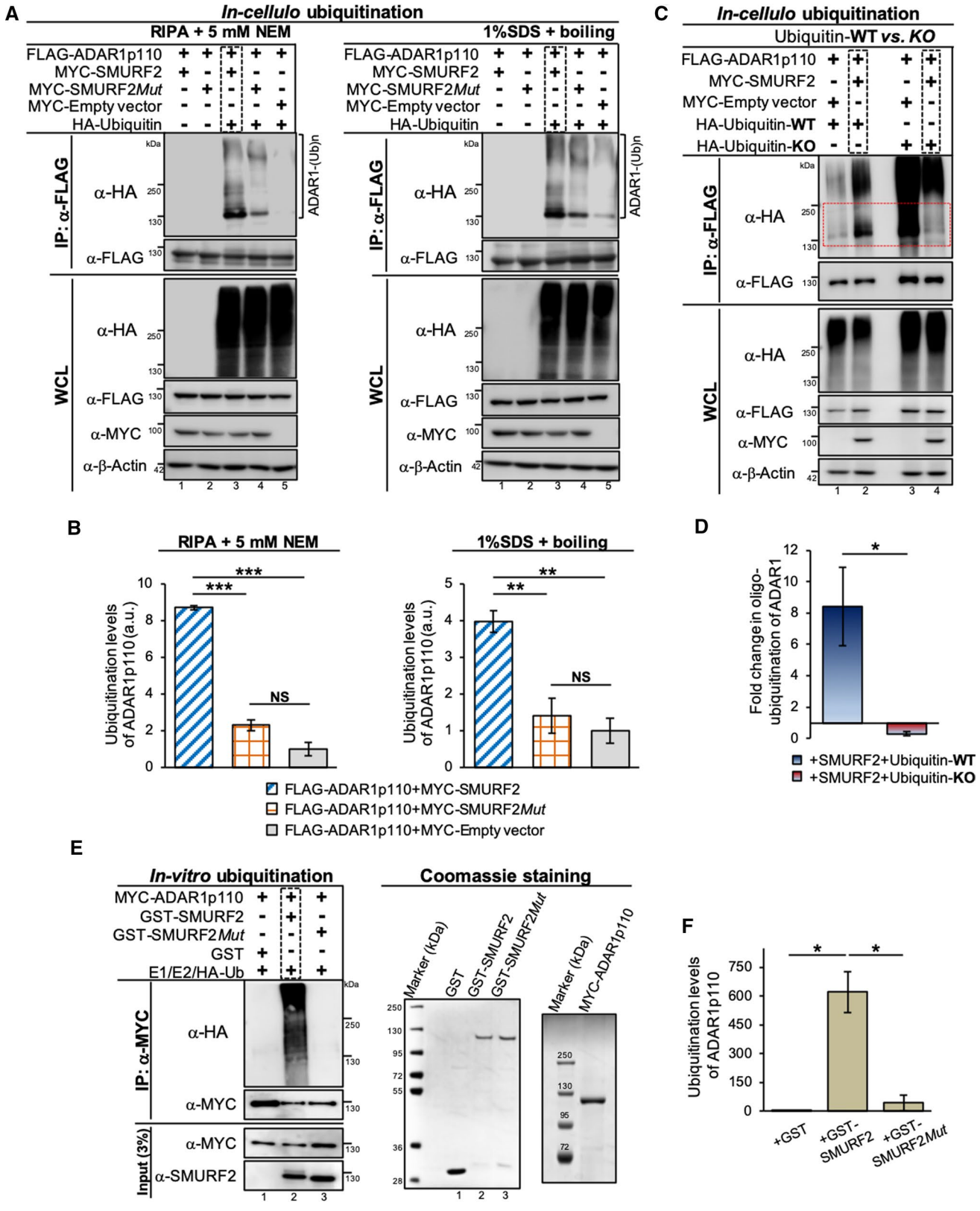

tissues of *Smurf2*KO and WT mice, using Western blotting and IHC analysis. The results (Fig. 3H, I and Supplementary Fig. 3G) revealed that, similar to SMURF2 knockdown cells, the decreased protein levels of ADAR1p110 are characteristic of *Smurf2*-ablated tissues. Furthermore, IHC analysis conducted on human tissue samples (TMAs) pointed to a

◂**Fig. 2** SMURF2 ubiquitinates ADAR1p110 in a direct manner. **A** Western blot analysis of in cellulo ubiquitination assays conducted in HEK-293T cells under different cell lysis conditions. **B** Quantification of data on the effects of SMURF2 on ADAR1 ubiquitination shown in **A** obtained in three independent experiments. Data are mean ± SEM. ***$P \leq 0.001$, ****$P \leq 0.0001$. **C** In cellulo ubiquitination assay showing the disappearance of SMURF2-mediated oligoubiquitination of ADAR1 (marked in the red box) in HEK-293T cells coexpressing HA-Ubiquitin-KO mutant. **D** Quantification of the data shown in **C** obtained in four different experiments. The intensity of oligo-ubiquitinated ADAR1 was normalized to the intensity of FLAG-ADAR1p110 in the IP samples and calculated as a fold change relatively the corresponding controls. Data are mean ± SEM. *$P \leq 0.05$. **E** In vitro ubiquitination of MYC-ADAR1p110 by GST-SMURF2. MYC-ADAR1p110 was pulled-down from the reaction using anti-MYC antibody. Coomassie blue gel staining on the right shows GST, GST-SMURF2 (active and mutant) and MYC-ADAR1p110 proteins used in the study. **F** Quantification of the data shown in **E** from two separate experiments. The ubiquitination levels of MYC-ADAR1p110 were normalized to its levels in the IP samples. Data are mean ± SEM. *$P \leq 0.05$

positive reciprocal relationship between the expression of SMURF2 and ADAR1, with Spearman's rho (rs) = 0.356 and P value < 0.0001. This relationship was particularly notable in the spleen, kidney, intestine, lymph nodes, salivary and thyroid glands and adenohypophysis (Supplementary Fig. 3H and Table 3). In all these tissues, a higher expression of SMURF2 was associated with a higher expression of ADAR1, and vice versa: tissues which exhibited a lower expression of SMURF2 showed lower levels of ADAR1. Overall, the TMA analysis showed that 63% of human tissues exhibit an interrelatedness between SMURF2 and ADAR1 expression (Supplementary Fig. 3I).

SMURF2 regulates ADAR1 stability through K744 residue

To further investigate the mechanism underlying the SMURF2-mediated stabilization of ADAR1, we mapped on ADAR1 the sites of SMURF2-mediated ubiquitination. To this end, we performed an in cellulo ubiquitination assay with subsequent pull-down of ADAR1p110 and enrichment of its ubiquitinated peptides using the PTMScan K-ε-GG immunoaffinity approach [40]. The samples were then analyzed in MS (Supplementary Fig. 4A). Using this approach, we identified on ADAR1 thirteen lysine residues as potential ubiquitination sites of SMURF2 (out of 76 lysines residues present in ADAR1p110) (Fig. 4A and Supplementary Fig. 4B). To determine which of the identified ADAR1 residues are true ubiquitin acceptors of SMURF2, we mutated each of these lysines to arginine (K-to-R mutation) and analyzed the ability of SMURF2 to ubiquitinate these ADAR1 mutants using an in cellulo ubiquitination assay. The results (Fig. 4B, C, upper panel) showed that the ubiquitination of two particular ADAR1 mutants, K296R and K744R, was considerably reduced in comparison to ADAR1-WT, with a more significant decrease in the ubiquitination levels of K744R ($P = 0.002$ for K744R and $P = 0.048$ for K296R). The data also showed that the expression levels of ADAR1p110-K744R were significantly decreased in comparison to ADAR1-WT or to any other analyzed K-to-R mutant or mutant combinations not involving K744R (Fig. 4C–E). CLSM analysis also showed a diminished protein expression of ADAR1-K744R in different types of cells (Fig. 4F, G). Moreover, we found that the reduced protein levels of ADAR1-K744R can be restored by the inhibition of cell proteolytic machineries with proteasomal and lysosomal inhibitors (Fig. 4H, I and Supplementary Fig. 4C), supporting our other findings on the posttranslational mode of ADAR1 regulation by SMURF2. This conclusion was further supported by cycloheximide (CHX) experiments, which showed a significantly increased turnover of ADAR1-K744R versus its wild-type counterpart (Fig. 4J, K and Supplementary Fig. 4D).

SMURF2-insensitive ADAR1-K744R mutant is enzymatically incompetent

The protein sequence alignments of different animal species conducted using Clustal Omega [57] revealed that the K744 residue of ADAR1p110 is highly conserved (Supplementary Fig. 5A). Moreover, the protein variation effect analyzer (PROVEAN, [58]) indicated that K744 mutation to arginine may have a deleterious effect on ADAR1 function (Supplementary Fig. 5B). To experimentally test this possibility, we first analyzed the ability of ADAR1-K744R to edit the filamin B (*FLNB*) gene transcript—one of the major ADAR1p110 editing targets in human cells [59, 60]. The analysis was conducted in HEK-293T cells, which have a low A-to-I editase activity [50, 61, 62] due to enhanced degradation of ADAR1, preventable by inhibition of the proteasomal and lysosomal degradation pathways (Supplementary Fig. 4C). HEK-293T cells were transfected with either FLAG-ADAR1p110-WT or K744R mutant and their RNA extracted 24 and 48 h later. Cells transfected with enzymatically inactive FLAG-ADAR1 (ADAR1p110-H615Q/E617A), ADAR1p110-K296R or an empty FLAG vector served as additional controls. RNA was then reverse-transcribed and, following treatment with DNase I, amplified with primers flanking the *FLNB* editing site (c.A6805G:pM2269V). A-to-I editing of *FLNB* was then assessed using Sanger sequencing. The results (Fig. 5A–C and Supplementary Fig. 5C) show that enforced expression of ADAR1p110-WT significantly increased the editing levels of *FLNB*, both 24 and 48 h after transfection, with a more prominent effect at 48 h. They also show that K744R, but not K296R mutant, failed to edit the *FLNB* transcript, similar to the catalytically inactive ADAR1p110 (H615Q/

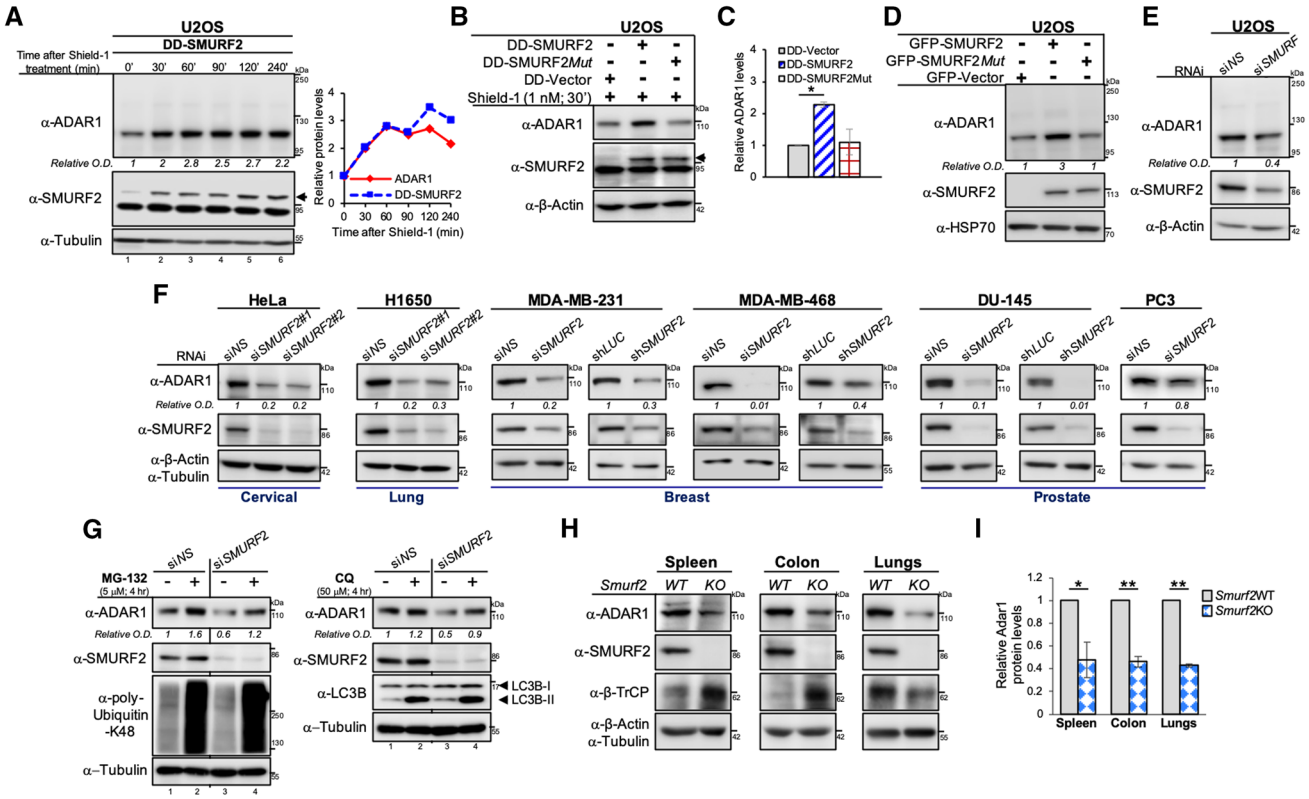

Fig. 3 SMURF2 stabilizes ADAR1p110 in an E3 ubiquitin ligase-dependent manner. **A** Immunoblot analysis showing the effect of the induction of DD-SMURF2 (arrow-labeled) with Shield-1 on ADAR1p110 expression in U2OS cells. Cells were treated with 1 nM of Shield-1 for the indicated period/s of time. The quantification of the relative protein levels of ADAR1p110 and DD-SMURF2 at different time-points after Shield-1 treatment is shown on the right. **B** Western blot analysis showing the dependence of the phenomenon shown in **A** on the unaltered catalytic activity of SMURF2. Cells were treated with 1 nM of Shield-1 for 30 min. The arrow shows the induced wild-type and mutant forms of DD-SMURF2. **C** Quantification of data shown in **B** from two separate experiments. Data are mean ± SEM. $*P \leq 0.05$. **D** Western blot analysis showing that overexpression of catalytically active GFP-SMURF2, but not its E3 ligase-dead form GFP-SMURF2*Mut*, increases ADAR1p110 protein levels. **E** *SMURF2* knockdown diminishes protein levels of ADAR1p110. **F** Western blot analysis showing the effect of SMURF2 knockdown on the steady-state levels of ADAR1p110 in different types of cells. Non-silencing siRNA (siNS) and shRNA directed against Luciferase (shLuc) were used as controls for siRNA and shRNA experiments, respectively. **G** Immunoblot analysis of ADAR1 protein expression in SMURF2 knockdown PC3 cells after treatment with MG-132 (5 μM; 4 h) and chloroquine, CQ (50 μM; 4 h). Inhibition of the proteasomal and lysosomal degradation pathways was verified using anti-poly-ubiquitin-K48 and anti-LC3B antibodies, respectively. **H** Western blot analysis of ADAR1 expression in *Smurf2*-depleted and wild-type mouse tissues. The expression levels of the SCF subunit β-TrCP were also examined (explained in the "Discussion" section). **I** The quantification of data on the effect of SMURF2 on ADAR1 shown in **G** obtained on three different pairs of mice. Data are mean ± SEM. $*P \leq 0.05$, $**P \leq 0.01$

E617A). Similar results were also obtained in HeLa cells, where, in addition to *FLNB*, we also examined the editing of antizyme inhibitor 1 (*AZIN1*), another established RNA-editing target of ADAR1p110 [18]. In both cases, ADAR1-K744R mutant was incapable of editing these transcripts and showed results highly similar to the enzymatically dead ADAR1p110-H615Q/E617A (Fig. 5D–F and Supplementary Fig. 5D). The analysis of mouse tissues also showed that RNA editing of ADAR1p110 transcript substrates was substantially decreased in *Smurf2*KO tissues (Supplementary Fig. 5E).

To clarify whether the reduced editase activity of ADAR1p110-K744R emanates from its decreased expression, we forcibly expressed ADAR1p110-K744R at a level similar to ADAR1-WT (cells were transfected at a threefold excess of ADAR1-K744R versus ADAR1-WT). The results (Fig. 5G–I) showed that even when ADAR1p110-K744R mutant was expressed at a level similar to ADAR1-WT (Fig. 5H, lanes 4 vs. 2 and 8 vs. 6) it was incapable of editing its RNA transcript target (Fig. 5G, I), suggesting that ADAR1p110-K744R is enzymatically incompetent.

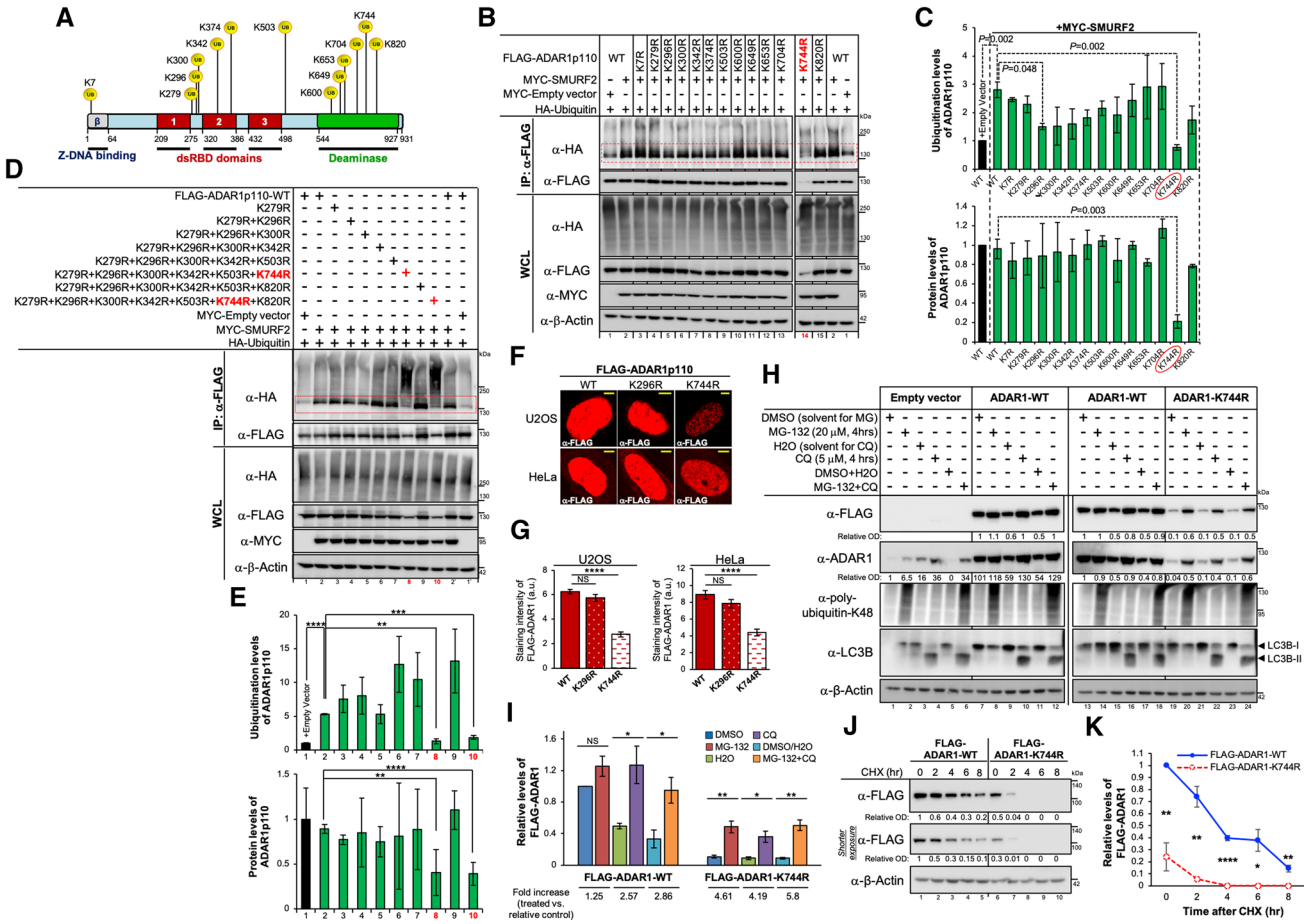

Fig. 4 Mapping on ADAR1 of SMURF2 ubiquitination sites and identification of K744 as a residue essential for ADAR1 stability maintenance. **A** Schematic diagram showing the position of identified lysine residues of ADAR1p110 as ubiquitination sites of SMURF2. **B** Western blot analysis showing the effects of K-to-R mutations of ADAR1p110 on its ubiquitination and expression levels in HEK-293T cells. **C** Quantification of the data shown in **B** from several independent experiments. The data for ADAR1-WT and K744R mutant were collected from three independent experiments; the experiments with all other listed mutants were performed twice. Data are mean ± SEM. **D** Western blot analysis of in cellulo ubiquitination assay conducted with different ADAR1 mutant combinations. **E** Quantification of the data described in **D** derived from three independent experiments. Data are mean ± SEM. **F** Confocal microscopy images showing expression of ADAR1-WT, ADAR1-K296R and ADAR1-K744 mutants in U2OS and HeLa cells. Scale bar: 5 µm. **G** Quantification of the data shown in **F** collected on 50–52 cells per sample. Data are mean ± SEM. $^{****}P \leq 0.0001$. *NS* nonsignificant. **H** Western blot analysis showing that degradation of ADAR1-K744R can be rescued through the inhibition of its proteasomal and lysosomal turnover, using MG-132 and CQ treatments, respectively. Inhibition of the proteasomal and lysosomal degradation pathways were verified using anti-poly-ubiquitin-K48 and anti-LC3B antibodies, respectively. HEK-293T cells. **I** Quantification of the data described in **H** from three independent experiments. Data are mean ± SEM. $^{*}P \leq 0.05$, $^{**}P \leq 0.01$. **J** Western blot analysis showing protein turnover of ADAR1-WT and ADAR1-K744R in cycloheximide (CHX)-treated HEK-293T cells. CHX was administered to cells at a concentration of 50 µg/ml for the indicated period/s of time. **K** Quantification of the data described in **J** obtained in three independent experiments. Data are mean ± SEM. $^{*}P \leq 0.05$, $^{**}P \leq 0.01$, $^{****}P \leq 0.0001$. The expression levels (relative ODs) of ADAR1-WT and ADAR1-K744R were normalized to β-actin and calculated relatively to untreated ADAR1-WT control (lane 1). These values were also calculated relatively to each of the untreated controls: WT and K744R (shown in Supplementary Fig. 4D)

SMURF2 regulates ADAR1 interactome, influencing its stability and functions

To analyze the impact of SMURF2 on ADAR1 on a global scale, we then assessed the effects of SMURF2 expression on ADAR1 protein–protein interactions, using a workflow shown in Supplementary Fig. 6. We found that ADAR1 interacted with a similar number of proteins in MYC-SMURF2-expressing and control cells: 735 proteins in the MYC-SMURF2-expressing cells and 736 proteins in the control group (FDR ≤ 1%). Seven hundred proteins were shared by both groups (Fig. 6A, left panel). After applying an additional threshold of a twofold change in protein abundance, we found that SMURF2 increased the abundance of 80 ADAR1 interactors, while decreasing it for 74 proteins (Fig. 6A, right panel). The subsequent characterization of

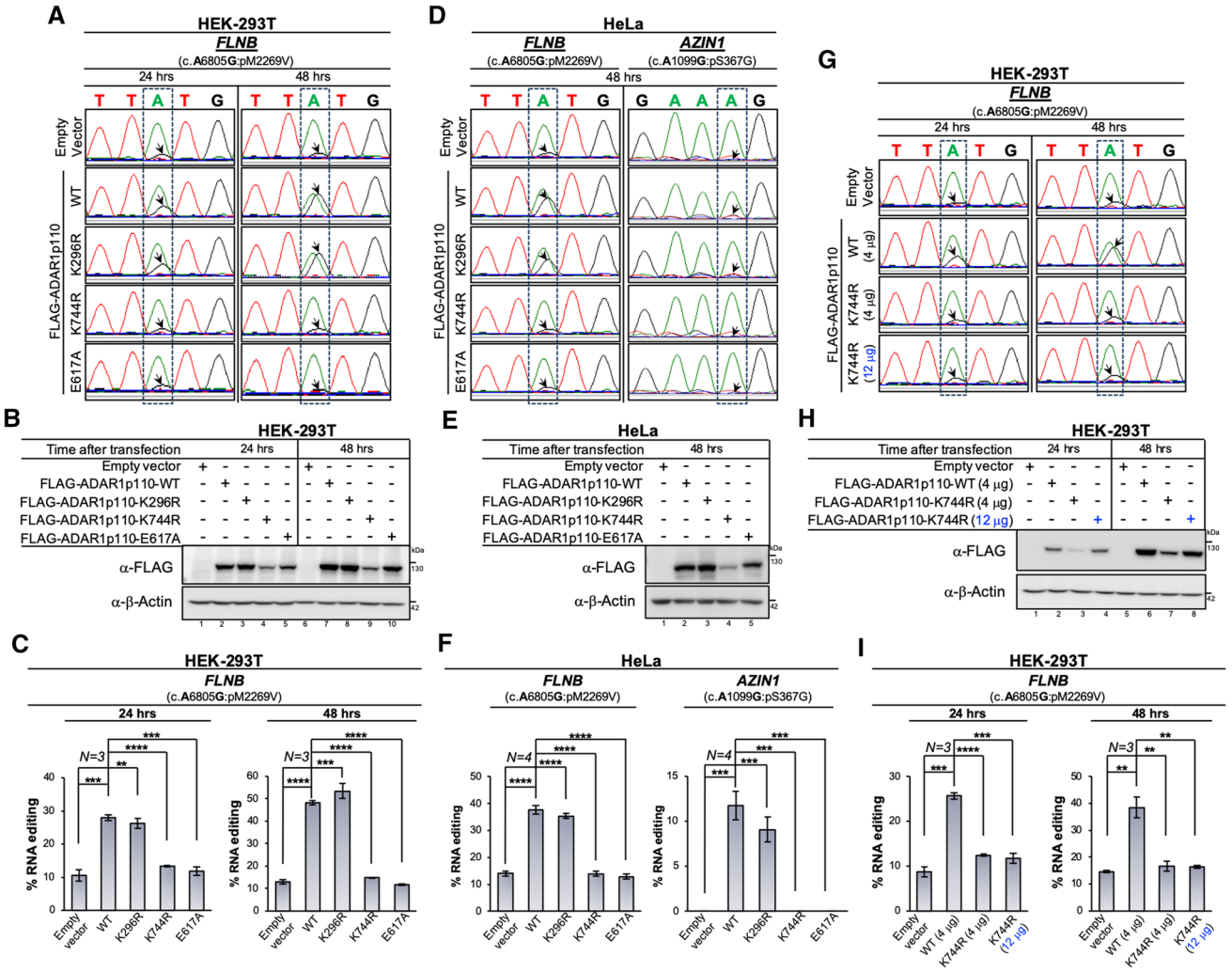

Fig. 5 SMURF2-insensitive ADAR1-K744R mutant is enzymatically incompetent. **A** Sanger sequencing chromatograms showing the efficiency of RNA editing of the *FLNB* transcript in HEK-293T cells 24 and 48 h after cell transfection with the indicated vectors and constructs. Note that, in the chromatograms, the editing site appears as mixed A and G peaks. The edited position is indicated by arrows. **B** Western blot analysis showing expression of ADAR1p110-WT and its K296R, K744R and enzymatically inactive mutants (H615Q/E617A, denoted as E617A) 24 and 48 h after cell transfection. The data are related to the results described in **A**. **C** Quantification of RNA editing of *FLNB* transcript described in **A** obtained from three independent experiments. Data are mean ± SEM. $^{**}P \leq 0.01$, $^{***}P \leq 0.001$, $^{****}P \leq 0.0001$. **D** Sanger sequencing chromatograms showing RNA editing of *FLNB* and *AZIN1* in HeLa cells 48 h after cell transfection. **E** Western blot analysis showing expression of ADAR1-WT and its mutants in HeLa cells. **F** Quantification of the data on RNA editing of *FLNB* and *AZIN1* transcripts in HeLa cells obtained from four independent experiments. Data are mean ± SEM. $^{***}P \leq 0.001$, $^{****}P \leq 0.0001$. **G** Sanger sequencing chromatograms showing the efficiency of *FLNB* editing 24 and 48 h after cell transfection with either equal amounts of ADAR1 (4 µg for both WT and K744R) or at the threefold increase of ADAR1-K744R mutant (4 µg for WT and 12 µg for K744R) to equalize expression of K744R to its WT counterpart. **H** Immunoblot analysis showing expression levels ADAR1-WT and ADAR1-K744R described in **G**. **I** Quantification of the data on RNA editing of *FLNB* transcript described in (G and H) obtained from three independent experiments. Data are Mean ± SEM. $^{**}P \leq 0.01$, $^{***}P \leq 0.001$, $^{****}P \leq 0.0001$

ADAR1 binding partners upregulated by SMURF2 revealed that these proteins are functional in nucleic acid binding (32.6%), transcription regulation (20.9%), protein modification (11.6%), cytoskeleton organization (9.3%) and metabolite interconversion (7%) (Fig. 6B, top panel). The downregulated proteins included the metabolite interconversion enzymes (27.3%), nucleic acid binding proteins (18.2%), protein modifying enzymes (11.4%), scaffolds/adaptors (11.4%), translational (9.1%) and cytoskeletal (6.8%) proteins (Fig. 6B, bottom panel).

The localization analysis of ADAR1 interactors affected by SMURF2 showed that most of these proteins are sequestered in the nucleus, although some ADAR1 binding partners could also be found in the cytoplasm, endoplasmic reticulum, mitochondria, centrosome and membrane (Fig. 6C). This localization of ADAR1p110 interactors is in

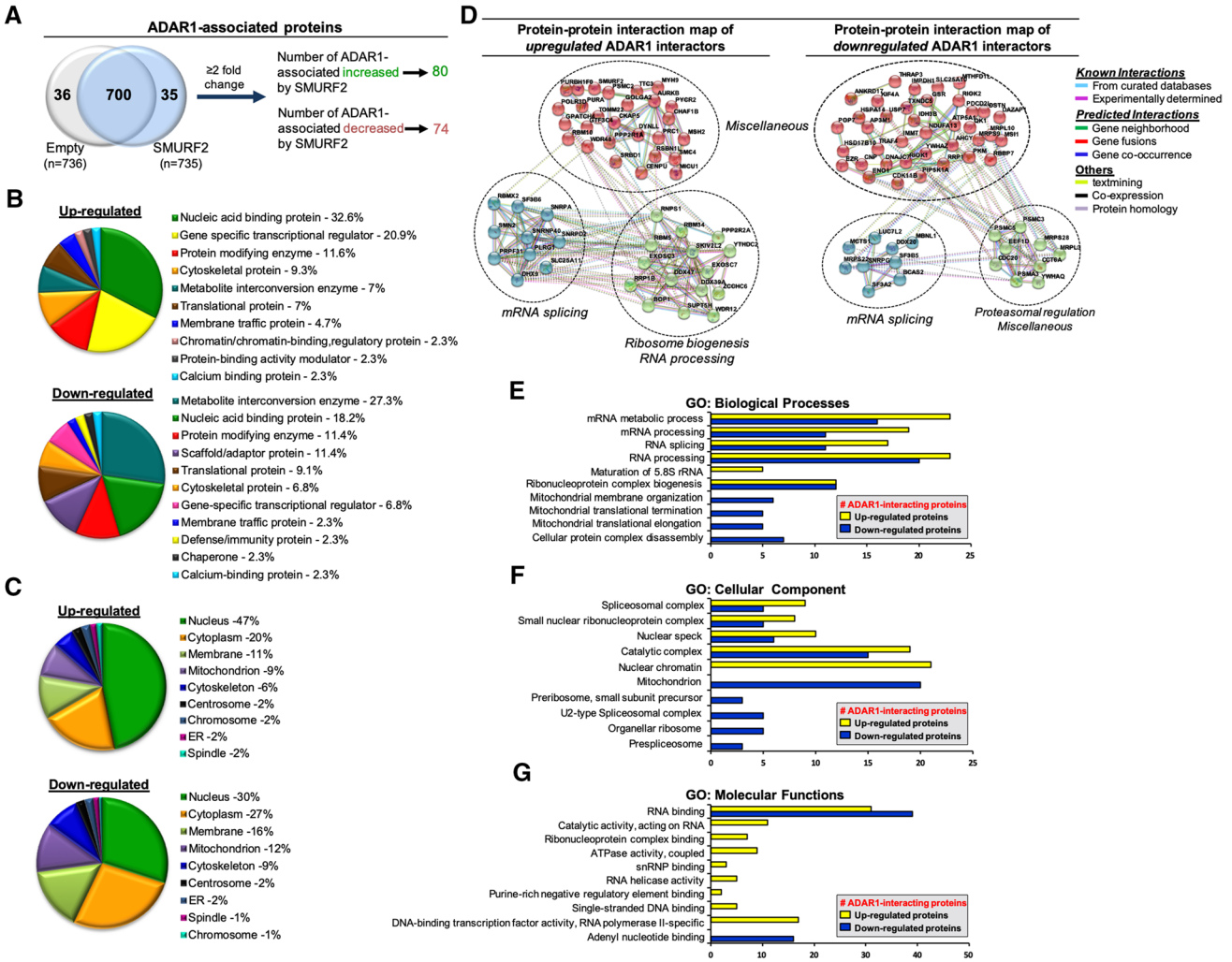

Fig. 6 SMURF2 regulates ADAR1 protein–protein interactions and functions. **A** Venn diagram showing the total number of ADAR1-associated proteins identified by LC–MS/MS in HEK-293T cells expressing either MYC-SMURF2 or Empty-MYC vector. **B** Protein classes of ADAR1-interacting partners, whose abundance was either increased or decreased by SMURF2 using the PANTHER classification system. **C** The cellular localization of ADAR1-associated proteins affected by SMURF2 (using the UniProtKB tool). ER, endoplasmic reticulum. **D** Protein–protein interaction network of the ADAR1 interactome obtained using STRING 11.0 platform. Only the interactors connected within the network are shown. Proteins are indicated by nodes labeled with the encoding gene symbol. Clusters identified by k-means clustering are shown in different colors. **E–G** GO enrichment analysis of biological processes, cellular components and molecular functions of ADAR1-interacting proteins enriched by SMURF2. Note that only the top 10 enriched functions and processes are shown (the detailed data are presented in Supplementary Table 4). GO terms were considered significant when they showed Benjamini and Hochberg adjusted FDR (q-value FDR B&H) < 0.05

agreement with previous findings showing that ADAR1p110 interactome comprises both nuclear and cytoplasm-sequestered proteins and organelles [63].

Further reconstruction of ADAR1 protein–protein interactions affected by SMURF2 showed its effect on molecular networks regulating mRNA splicing, ribosome biogenesis and RNA processing (Fig. 6D). Notably, in this analysis, we found that the forced expression of SMURF2 decreased ADAR1 associations with the regulators of proteasomal degradation, which is in line with our other findings on the protective role of SMURF2 against ADAR1 proteolysis. The GO enrichment analysis of biological process modified by SMURF2 also showed that SMURF2 affects the interaction of ADAR1 with proteins involved in RNA metabolism, processing, splicing, rRNA maturation, ribonucleoprotein (RNP) complex biogenesis and protein complex disassembly (Fig. 6E and Supplementary Table 4). Furthermore, the GO cellular components analysis revealed that SMURF2 modulates ADAR1 associations with proteins implicated in the formation of spliceosomal and small nuclear RNP (snRNP) complexes, catalytic complexes, nuclear speck and chromatin (Fig. 6F).

Finally, the GO analysis of molecular functions of ADAR1's interactors affected by SMURF2 showed that SMURF2 enriches the association of ADAR1 with proteins implicated in the regulation of catalytic activity acting on RNA, snRNP and RNP complex binding, ATPase activity, and RNA helicase activity (Fig. 6G).

Discussion

ADAR1 is increasingly recognized as a critical player in the regulation of RNA expression, structure and function. Thus, it is not surprising that ADAR1 is implicated in the regulation of diverse molecular processes and exhibits a multitude of effects on cellular functions both under physiological conditions and in the disease states, including cancer. Despite the strong linkage of ADAR1 to different physiological and pathobiological conditions, the regulatory mechanisms governing its protein expression and activity, particularly of its constitutively expressed ADAR1p110 form, are poorly understood. The results of the current research show that the E3 ubiquitin ligase SMURF2 operates as a pivotal regulator of ADAR1p110. We show that SMURF2 directly interacts with ADAR1p110, independently of SMURF2 catalytic status, oligo-ubiquitinates it in a SMURF2 E3 ligase-dependent manner and stabilizes ADAR1p110 protein expression by reducing its proteolysis through the proteasomal and lysosomal degradation pathways (Figs. 1, 2, 3 and Supplementary Figs. 1 and 2). Both of these pathways were found in our study to regulate the cellular abundance of ADAR1p110 (Figs. 3A, 4H). One possible explanation for this phenomenon could be the formation on ADAR1p110 of heterotypic ubiquitin chains, which were influenced by SMURF2 (Supplementary Fig. 2B). These chains may be less recognizable by the proteolytic machineries, leading to the stabilization of ADAR1p110. Indeed, SMURF2 has been shown to interfere with both proteasomal and autophagic-lysosomal degradation of its protein substrates by modifying their ubiquitination status [33]. Further investigation of a link between ADAR1 heterotypic ubiquitination and its protection from proteolysis is needed to clarify this phenomenon. The ability of SMURF2 to positively regulate ADAR1p110 was observed in different types of human cells and tissues, as well as in mouse tissues derived from *Smurf2*KO and control WT animals, suggesting SMURF2 as a physiological regulator of ADAR1p110 (Fig. 3 and Supplementary Fig. 3). This finding is further supported by the results showing that the efficiency of RNA editing catalyzed by ADAR1p110 is substantially diminished in *Smurf2*-ablated mouse tissues (Supplementary Fig. 5E).

Next, using a set of ubiquitination and mutagenesis analyses, we demonstrated that SMURF2 ubiquitinates ADAR1p110 at K744 residue (Fig. 4 and Supplementary Fig. 4A, B). This residue is located in the deaminase domain of ADAR1p110 and corresponds to the K1039 residue of an IFN-inducible ADAR1p150. Interestingly, the mutation of ADAR1p110-K744 to arginine (c.2231A>G, p.K744R), or ADAR1p150-K1039 to arginine (c.3116A>G, p.K1039R) have been reported in different human disorders, including DSH [64] and cancer [65, 66]. Furthermore, because K744 is located in ADAR1p110's catalytic domain, and in light of the high conservation of this site among different animal species (Supplementary Fig. 5A), we hypothesized that the K744R mutation would compromise the functionality of ADAR1p110. This possibility was also suggested by the PROVEAN analysis, which indicated that the K-to-R mutation of ADAR1p110 at K744 could lead to a dramatic change in ADAR1's function (Supplementary Fig. 5B). In agreement with this prediction, our experimental findings show that both the protein stability and activity of ADAR1p110-K744R are profoundly affected (Figs. 4, 5). In fact, the catalytic activity of ADAR1p110-K744R was reduced to the level of the deaminase-deficient ADAR1p110 (H615Q/E617A)—a phenomenon that has been consistently observed in different types of human cells, using *FLNB* and *AZIN1* transcripts as ADAR1 endogenous substrates. Notably, the results also showed that the forced expression of the K744R mutant at a level similar to ADAR1-WT did not increase RNA editing as compared to ADAR1-WT (Fig. 5G–I), suggesting that K744R mutation represses ADAR1 activity, in addition to diminishing its expression levels. In future studies, it would be interesting to examine the effect of K744R mutation on the RNA editing of other ADAR1 transcript targets, including protein coding and non-coding RNAs, and to unravel the biological effects of this mutation in animal models.

The conducted proteome interaction network analysis also pointed to SMURF2 as a pivotal regulator of ADAR1, affecting its interactions with proteins involved in RNA metabolic processes, RNA processing, nucleic acids binding, transcription regulation, and protein modifications (Fig. 6). Interestingly, the interactions of ADAR1 with molecular factors associated with proteasomal degradation were diminished by SMURF2 (Fig. 6D), supporting our other findings on SMURF2 as a positive regulator of ADAR1. Note that, in the MS analysis, we found many previously reported ADAR1 interactors (e.g., DICER1, DHX9, ILF2, ILF3 and nucleolin, among others) [62, 67, 68], supporting the validity of the results obtained in this study. Taken together, these findings suggest SMURF2 as a key cellular factor influencing the protein expression, interactions and function of ADAR1p110.

There are several possible scenarios for how SMURF2, which is primarily known to promote the degradation of its protein substrates [33, 69], protects ADAR1p110 from the proteolysis. First, as described above, SMURF2, through direct binding and ubiquitination of ADAR1, modifies its

ubiquitinating status, which may reduce the detection of ADAR1 by the proteolytic machineries. Second, SMURF2-mediated ubiquitination may lead to conformational changes in ADAR1, rendering it less approachable/recognizable by degradation-promoting E3s, e.g., by $SCF^{\beta TrCP}$ [28]. As a result, ADAR1 would be stabilized and its cellular levels increased. The targeted regulation by SMURF2 of E3 ligases promoting ADAR1 degradation, for example of β-TrCP [70], is also possible. This possibility is partially supported by our results showing that protein levels of β-TrCP are increased in certain *Smurf2*KO tissues (Fig. 3H and Supplementary Fig. 7). Third, SMURF2-dependent stabilization of ADAR1 may involve binding to ubiquitinated ADAR1 of deubiquitinating enzymes (DUBs), acting in a tandem with SMURF2 in the regulation of its protein substrates. This mode of the regulation was, for example, reported in the regulation of TGF-β family signaling by SMURF2 and two ubiquitin-specific peptidases USP4 and USP15 [71, 72]. It is also possible that SMURF2 regulates ADAR1p110 by modulating the expression levels and/or activities of both DUBs and E3s. Finally, another layer in the SMURF2-mediated regulation of ADAR1 may be imposed by the upstream signaling pathways, e.g., mediated by AKT. Indeed, this serine–threonine protein kinase has been shown to phosphorylate and suppress both ADAR1 [26] and SMURF2 [36, 73].

Supplementary Information The online version contains supplementary material available at https://doi.org/10.1007/s00018-022-04272-8.

Acknowledgements We are thankful to Profs. Gideon Rechavi and Gal Markel for providing ADAR1p110 wild-type and catalytically inactive constructs, as well as to other investigators who shared with use their reagents. We are also grateful to Basem Hijazi for helping with the statistical data analysis.

Author contributions PK, VNK, DMA, AE and GLC performed experiments and analyzed the data. In addition, VNK and GLC carried out all experiments during the manuscript revision. BP analyzed and scored the TMAs. MB and PK designed the research strategy and experimental plan. MB conceived the study, supervised the project, and wrote the article.

Funding This work was supported by the Dayan Foundation and Israel Science Foundation (#422/20).

Data availability The datasets generated during and/or analyzed during the current study are available in the ProteomeXchange Consortium via the PRIDE [74] partner repository with the dataset identifiers PXD025325 (ADAR1 ubiquitination sites) and PXD025338 (ADAR1 interactome).

Code availability Not applicable.

Declarations

Conflict of interest The authors declare no conflict of interest.

Ethics approval Animal protocols were approved by the Animal Care and Use Committee of BIU.

Consent to participate Not applicable.

Consent for publication Not applicable.

References

1. Savva YA, Rieder LE, Reenan RA (2012) The ADAR protein family. Genome Biol 13(12):252
2. Fritzell K, Xu LD, Lagergren J, Öhman M (2018) ADARs and editing: the role of A-to-I RNA modification in cancer progression. Semin Cell Dev Biol 79:123–130
3. Nishikura K (2016) A-to-I editing of coding and non-coding RNAs by ADARs. Nat Rev Mol Cell Biol 17(2):83–96
4. Baysal BE, Sharma S, Hashemikhabir S, Janga SC (2017) RNA editing in pathogenesis of cancer. Cancer Res 77(14):3733–3739
5. Peng X, Xu X, Wang Y, Hawke DH, Yu S, Han L, Zhou Z, Mojumdar K, Jeong KJ, Labrie M et al (2018) A-to-I RNA editing contributes to proteomic diversity in cancer. Cancer Cell 33(5):817-828.e7
6. Tang SJ, Shen H, An O, Hong H, Li J, Song Y, Han J, Tay DJT, Ng VHE, Bellido Molias F et al (2020) Cis- and trans-regulations of pre-mRNA splicing by RNA editing enzymes influence cancer development. Nat Commun 11(1):799
7. Eisenberg E, Levanon EY (2018) A-to-I RNA editing—immune protector and transcriptome diversifier. Nat Rev Genet 19(8):473–490
8. Ahmad S, Mu X, Yang F, Greenwald E, Park JW, Jacob E, Zhang CZ, Hur S (2018) Breaching self-tolerance to Alu duplex RNA underlies MDA5-mediated inflammation. Cell 172(4):797-810.e13
9. Chung H, Calis JJA, Wu X, Sun T, Yu Y, Sarbanes SL, Dao Thi VL, Shilvock AR, Hoffmann HH, Rosenberg BR et al (2018) Human ADAR1 prevents endogenous RNA from triggering translational shutdown. Cell 172(4):811-824.e14
10. Shiromoto Y, Sakurai M, Qu H, Kossenkov AV, Nishikura K (2020) Processing of *Alu* small RNAs by DICER/ADAR1 complexes and their RNAi targets. RNA 26(12):1801–1814
11. Orecchini E, Doria M, Antonioni A, Galardi S, Ciafrè SA, Frassinelli L, Mancone C, Montaldo C, Tripodi M, Michienzi A (2017) ADAR1 restricts LINE-1 retrotransposition. Nucleic Acids Res 45(1):155–168
12. Patterson JB, Samuel CE (1995) Expression and regulation by interferon of a double-stranded-RNA-specific adenosine deaminase from human cells: evidence for two forms of the deaminase. Mol Cell Biol 15(10):5376–5388
13. Strehblow A, Hallegger M, Jantsch MF (2002) Nucleocytoplasmic distribution of human RNA-editing enzyme ADAR1 is modulated by double-stranded RNA-binding domains, a leucine-rich export signal, and a putative dimerization domain. Mol Biol Cell 13(11):3822–3835
14. Fritz J, Strehblow A, Taschner A, Schopoff S, Pasierbek P, Jantsch MF (2009) RNA-regulated interaction of transportin-1 and exportin-5 with the double-stranded RNA-binding domain regulates nucleocytoplasmic shuttling of ADAR1. Mol Cell Biol 29(6):1487–1497
15. Sakurai M, Shiromoto Y, Ota H, Song C, Kossenkov AV, Wickramasinghe J, Showe LC, Skordalakes E, Tang HY, Speicher DW et al (2017) ADAR1 controls apoptosis of stressed cells by inhibiting Staufen1-mediated mRNA decay. Nat Struct Mol Biol 24(6):534–543

16. Sun T, Yu Y, Wu X, Acevedo A, Luo JD, Wang J, Schneider WM, Hurwitz B, Rosenberg BR, Chung H et al (2021) Decoupling expression and editing preferences of ADAR1 p150 and p110 isoforms. Proc Natl Acad Sci USA 118(12):e2021757118
17. Vesely C, Jantsch MF (2021) An I for an A: dynamic regulation of adenosine deamination-mediated RNA editing. Genes (Basel) 12(7):1026
18. Song B, Shiromoto Y, Minakuchi M, Nishikura K (2021) The role of RNA editing enzyme ADAR1 in human disease. Wiley Interdiscip Rev RNA 8:e1665
19. Shiromoto Y, Sakurai M, Minakuchi M, Ariyoshi K, Nishikura K (2021) ADAR1 RNA editing enzyme regulates R-loop formation and genome stability at telomeres in cancer cells. Nat Commun 12(1):1654
20. Yang CC, Chen YT, Chang YF, Liu H, Kuo YP, Shih CT, Liao WC, Chen HW, Tsai WS, Tan BC (2017) ADAR1-mediated 3 (UTR editing and expression control of antiapoptosis genes fine-tunes cellular apoptosis response. Cell Death Dis 8(5):e2833
21. Teoh PJ, An O, Chung TH, Chooi JY, Toh SHM, Fan S, Wang W, Koh BTH, Fullwood MJ, Ooi MG et al (2018) Aberrant hyperediting of the myeloma transcriptome by ADAR1 confers oncogenicity and is a marker of poor prognosis. Blood 132(12):1304–1317
22. Nemlich Y, Baruch EN, Besser MJ, Shoshan E, Bar-Eli M, Anafi L, Barshack I, Schachter J, Ortenberg R, Markel G (2018) ADAR1-mediated regulation of melanoma invasion. Nat Commun 9(1):2154
23. Ramírez-Moya J, Baker AR, Slack FJ, Santisteban P (2020) ADAR1-mediated RNA editing is a novel oncogenic process in thyroid cancer and regulates miR-200 activity. Oncogene 39(18):3738–3753
24. Kung CP, Cottrell KA, Ryu S, Bramel ER, Kladney RD, Bao EA, Freeman EC, Sabloak T, Maggi L Jr, Weber JD (2021) Evaluating the therapeutic potential of ADAR1 inhibition for triple-negative breast cancer. Oncogene 40(1):189–202
25. Tassinari V, Cesarini V, Tomaselli S, Ianniello Z, Silvestris DA, Ginistrelli LC, Martini M, De Angelis B, De Luca G, Vitiani LR et al (2021) ADAR1 is a new target of METTL3 and plays a pro-oncogenic role in glioblastoma by an editing-independent mechanism. Genome Biol 22(1):51
26. Bavelloni A, Focaccia E, Piazzi M, Raffini M, Cesarini V, Tomaselli S, Orsini A, Ratti S, Faenza I, Cocco L et al (2019) AKT-dependent phosphorylation of the adenosine deaminases ADAR-1 and -2 inhibits deaminase activity. FASEB J 33(8):9044–9061
27. Desterro JM, Keegan LP, Jaffray E, Hay RT, O'Connell MA, Carmo-Fonseca M (2005) SUMO-1 modification alters ADAR1 editing activity. Mol Biol Cell 16(11):5115–5126
28. Li L, Qian G, Zuo Y, Yuan Y, Cheng Q, Guo T, Liu J, Liu C, Zhang L, Zheng H (2016) Ubiquitin-dependent turnover of adenosine deaminase acting on RNA 1 (ADAR1) is required for efficient antiviral activity of type I interferon. J Biol Chem 291(48):24974–24985
29. Blank M, Tang Y, Yamashita M, Burkett SS, Cheng SY, Zhang YE (2012) A tumor suppressor function of Smurf2 associated with controlling chromatin landscape and genome stability through RNF20. Nat Med 18(2):227–234
30. Manikoth Ayyathan D, Koganti P, Marcu-Malina V, Litmanovitch T, Trakhtenbrot L, Emanuelli A, Apel-Sarid L, Blank M (2020) SMURF2 prevents detrimental changes to chromatin, protecting human dermal fibroblasts from chromosomal instability and tumorigenesis. Oncogene 39(16):3396–3410
31. Ramkumar C, Cui H, Kong Y, Jones SN, Gerstein RM, Zhang H (2013) Smurf2 suppresses B-cell proliferation and lymphomagenesis by mediating ubiquitination and degradation of YY1. Nat Commun 4:2598
32. Borroni AP, Emanuelli A, Shah PA, Ilić N, Apel-Sarid L, Paolini B, Manikoth Ayyathan D, Koganti P, Levy-Cohen G, Blank M (2018) Smurf2 regulates stability and the autophagic-lysosomal turnover of lamin A and its disease-associated form progerin. Aging Cell 17(2):e12732
33. Koganti P, Levy-Cohen G, Blank M (2018) Smurfs in protein homeostasis, signaling, and cancer. Front Oncol 8:295
34. Du C, Hansen LJ, Singh SX, Wang F, Sun R, Moure CJ, Roso K, Greer PK, Yan H, He Y (2019) A PRMT5-RNF168-SMURF2 axis controls H2AX proteostasis. Cell Rep 28(12):3199-3211.e5
35. Yu L, Dong L, Wang Y, Liu L, Long H, Li H, Li J, Yang X, Liu Z, Duan G et al (2019) Reversible regulation of SATB1 ubiquitination by USP47 and SMURF2 mediates colon cancer cell proliferation and tumor progression. Cancer Lett 448:40–51
36. Li Y, Yang D, Tian N, Zhang P, Zhu Y, Meng J, Feng M, Lu Y, Liu Q, Tong L et al (2019) The ubiquitination ligase SMURF2 reduces aerobic glycolysis and colorectal cancer cell proliferation by promoting ChREBP ubiquitination and degradation. J Biol Chem 294(40):14745–14756
37. Yu L, Dong L, Li H, Liu Z, Luo Z, Duan G, Dai X, Lin Z (2020) Ubiquitination-mediated degradation of SIRT1 by SMURF2 suppresses CRC cell proliferation and tumorigenesis. Oncogene 39(22):4450–4464
38. Emanuelli A, Borroni AP, Apel-Sarid L, Shah PA, Ayyathan DM, Koganti P, Levy-Cohen G, Blank M (2017) Smurf2-mediated stabilization of DNA topoisomerase IIα controls genomic integrity. Cancer Res 77(16):4217–4227
39. Nemlich Y, Greenberg E, Ortenberg R, Besser MJ, Barshack I, Jacob-Hirsch J, Jacoby E, Eyal E, Rivkin L, Prieto VG et al (2013) MicroRNA-mediated loss of ADAR1 in metastatic melanoma promotes tumor growth. J Clin Investig 123(6):2703–2718
40. Ilić N, Tao Y, Boutros-Suleiman S, Kadali VN, Emanuelli A, Levy-Cohen G, Blank M (2021) SMURF2-mediated ubiquitin signaling plays an essential role in the regulation of PARP1 PARylating activity, molecular interactions, and functions in mammalian cells. FASEB J 35(4):e21436
41. Manikoth Ayyathan D, Ilić N, Gil-Henn H, Blank M (2017) Generation of SMURF2 knockout human cells using the CRISPR/Cas9 system. Anal Biochem 531:56–59
42. Schindelin J, Arganda-Carreras I, Frise E, Kaynig V, Longair M, Pietzsch T, Preibisch S, Rueden C, Saalfeld S, Schmid B et al (2012) Fiji: an open-source platform for biological-image analysis. Nat Methods 9(7):676–682
43. Emanuelli A, Manikoth Ayyathan D, Koganti P, Shah PA, Apel-Sarid L, Paolini B, Detroja R, Frenkel-Morgenstern M, Blank M (2019) Altered expression and localization of tumor suppressive E3 ubiquitin ligase SMURF2 in human prostate and breast cancer. Cancers (Basel) 11(4):556
44. Vucenik I, Shamsuddin AM (2003) Cancer inhibition by inositol hexaphosphate (IP6) and inositol: from laboratory to clinic. J Nutr 133(11 Suppl 1):3778S-3784S
45. Silva EO, Bracarense AP (2016) Phytic acid: from antinutritional to multiple protection factor of organic systems. J Food Sci 81(6):R1357–R1362
46. Macbeth MR, Schubert HL, Vandemark AP, Lingam AT, Hill CP, Bass BL (2005) Inositol hexakisphosphate is bound in the ADAR2 core and required for RNA editing. Science 309(5740):1534–1539
47. Lamers MM, van den Hoogen BG, Haagmans BL (2019) ADAR1: "Editor-in-Chief" of cytoplasmic innate immunity. Front Immunol 10:1763
48. Levy-Cohen G, Blank M (2015) Functional analysis of protein ubiquitination. Anal Biochem 484:37–39
49. Emmerich CH, Cohen P (2015) Optimising methods for the preservation, capture and identification of ubiquitin chains and ubiquitylated proteins by immunoblotting. Biochem Biophys Res Commun 466(1):1–14
50. Anantharaman A, Gholamalamdari O, Khan A, Yoon JH, Jantsch MF, Hartner JC, Gorospe M, Prasanth SG, Prasanth KV

(2017) RNA-editing enzymes ADAR1 and ADAR2 coordinately regulate the editing and expression of Ctn RNA. FEBS Lett 591(18):2890–2904
51. Czermak P, Amman F, Jantsch MF, Cimatti L (2018) Organ-wide profiling in mouse reveals high editing levels of Filamin B mRNA in the musculoskeletal system. RNA Biol 15(7):877–885
52. Costa Cruz PH, Kato Y, Nakahama T, Shibuya T, Kawahara Y (2020) A comparative analysis of ADAR mutant mice reveals site-specific regulation of RNA editing. RNA 26(4):454–469
53. Mi H, Poudel S, Muruganujan A, Casagrande JT, Thomas PD (2016) PANTHER version 10: expanded protein families and functions, and analysis tools. Nucleic Acids Res 44(D1):D336–D342
54. Szklarczyk D, Morris JH, Cook H, Kuhn M, Wyder S, Simonovic M, Santos A, Doncheva NT, Roth A, Bork P et al (2017) The STRING database in 2017: quality-controlled protein-protein association networks, made broadly accessible. Nucleic Acids Res 45(D1):D362–D368
55. Chen J, Bardes EE, Aronow BJ, Jegga AG (2009) ToppGene Suite for gene list enrichment analysis and candidate gene prioritization. Nucleic Acids Res 37(Web Server issue):W305–W311
56. Bagchi S, Fredriksson R, Wallén-Mackenzie Å (2015) In situ proximity ligation assay (PLA). Methods Mol Biol 1318:149–159
57. Sievers F, Wilm A, Dineen D, Gibson TJ, Karplus K, Li W, Lopez R, McWilliam H, Remmert M, Söding J et al (2011) Fast, scalable generation of high-quality protein multiple sequence alignments using Clustal Omega. Mol Syst Biol 7:539
58. Choi Y, Chan AP (2015) PROVEAN web server: a tool to predict the functional effect of amino acid substitutions and indels. Bioinformatics 31(16):2745–2747
59. Qin YR, Qiao JJ, Chan TH, Zhu YH, Li FF, Liu H, Fei J, Li Y, Guan XY, Chen L (2014) Adenosine-to-inosine RNA editing mediated by ADARs in esophageal squamous cell carcinoma. Cancer Res 74(3):840–851
60. Chan TH, Lin CH, Qi L, Fei J, Li Y, Yong KJ, Liu M, Song Y, Chow RK, Ng VH et al (2014) A disrupted RNA editing balance mediated by ADARs (Adenosine DeAminases that act on RNA) in human hepatocellular carcinoma. Gut 63(5):832–843
61. Ohlson J, Pedersen JS, Haussler D, Ohman M (2007) Editing modifies the GABA(A) receptor subunit alpha3. RNA 13(5):698–703
62. Rossetti C, Picardi E, Ye M, Camilli G, D'Erchia AM, Cucina L, Locatelli F, Fianchi L, Teofili L, Pesole G et al (2017) RNA editing signature during myeloid leukemia cell differentiation. Leukemia 31(12):2824–2832
63. Hong H, An O, Chan THM, Ng VHE, Kwok HS, Lin JS, Qi L, Han J, Tay DJT, Tang SJ, Yang H, Song Y, Bellido Molias F, Tenen DG, Chen L (2018) Bidirectional regulation of adenosine-to-inosine (A-to-I) RNA editing by DEAH box helicase 9 (DHX9) in cancer. Nucleic Acids Res 46(15):7953–7969
64. Liu Q, Jiang L, Liu WL, Kang XJ, Ao Y, Sun M, Luo Y, Song Y, Lo WH, Zhang X (2006) Two novel mutations and evidence for haploinsufficiency of the ADAR gene in dyschromatosis symmetrica hereditaria. Br J Dermatol 154(4):636–642
65. Tate JG, Bamford S, Jubb HC, Sondka Z, Beare DM, Bindal N, Boutselakis H, Cole CG, Creatore C, Dawson E et al (2019) COSMIC: the Catalogue Of Somatic Mutations In Cancer. Nucleic Acids Res 47(D1):D941–D947
66. Cancer Genome Atlas Research Network (297 Collaborators) (2011) Integrated genomic analyses of ovarian carcinoma. Nature 474:609–615
67. Freund EC, Sapiro AL, Li Q, Linder S, Moresco JJ, Yates JR 3rd, Li JB (2020) Unbiased identification of trans regulators of ADAR and A-to-I RNA editing. Cell Rep 31(7):107656
68. Ota H, Sakurai M, Gupta R, Valente L, Wulff BE, Ariyoshi K, Iizasa H, Davuluri RV, Nishikura K (2013) ADAR1 forms a complex with Dicer to promote microRNA processing and RNA-induced gene silencing. Cell 153(3):575–589
69. Fu L, Cui CP, Zhang X, Zhang L (2020) The functions and regulation of Smurfs in cancers. Semin Cancer Biol 67(Pt 2):102–116
70. Shukla S, Allam US, Ahsan A, Chen G, Krishnamurthy PM, Marsh K, Rumschlag M, Shankar S, Whitehead C, Schipper M et al (2014) KRAS protein stability is regulated through SMURF2: UBCH5 complex-mediated β-TrCP1 degradation. Neoplasia 16(2):115–128
71. Zhou F, Xie F, Jin K, Zhang Z, Clerici M, Gao R, van Dinther M, Sixma TK, Huang H, Zhang L et al (2017) USP4 inhibits SMAD4 monoubiquitination and promotes activin and BMP signaling. EMBO J 36(11):1623–1639
72. Eichhorn PJ, Rodón L, Gonzàlez-Juncà A, Dirac A, Gili M, Martínez-Sáez E, Aura C, Barba I, Peg V, Prat A et al (2012) USP15 stabilizes TGF-β receptor I and promotes oncogenesis through the activation of TGF-β signaling in glioblastoma. Nat Med 18(3):429–435
73. Choi YH, Kim YJ, Jeong HM, Jin YH, Yeo CY, Lee KY (2014) Akt enhances Runx2 protein stability by regulating Smurf2 function during osteoblast differentiation. FEBS J 281(16):3656–3666
74. Perez-Riverol Y, Csordas A, Bai J, Bernal-Llinares M, Hewapathirana S, Kundu DJ, Inuganti A, Griss J, Mayer G, Eisenacher M et al (2019) The PRIDE database and related tools and resources in 2019: improving support for quantification data. Nucleic Acids Res 47(D1):D442–D450